RGB-D Salient Object Detection: A Survey

Tao Zhou, Deng-Ping Fan, Ming-Ming Cheng, Jianbing Shen, and Ling Shao

***Abstract*—Salient object detection (SOD), which simulates the human visual perception system to locate the most attractive object(s) in a scene, has been widely applied to various computer vision tasks. Now, with the advent of depth sensors, depth maps with affluent spatial information that can be beneficial in boosting the performance of SOD can easily be captured. Although various RGB-D based SOD models with promising performance have been proposed over the past several years, an in-depth understanding of these models and the challenges in this field remains lacking. In this paper, we provide a comprehensive survey of RGB-D based SOD models from various perspectives, and review related benchmark datasets in detail. Further, considering the fact that light fields can also provide depth maps, we review SOD models and popular benchmark datasets from this domain as well. Moreover, to investigate the SOD ability of existing models, we carry out a comprehensive evaluation and conduct an attribute-based evaluation of several representative RGB-D based SOD models. Finally, we discuss several challenges and open directions of RGB-D based SOD for future research. All collected models, benchmark datasets, source code links, datasets constructed for attribute-based evaluation, and codes for evaluation have been made publicly available at https://github.com/taozh2017/RGBD-SODsurvey.**

***Index Terms*—RGB-D based salient object detection, saliency detection, comprehensive evaluation, light fields.**

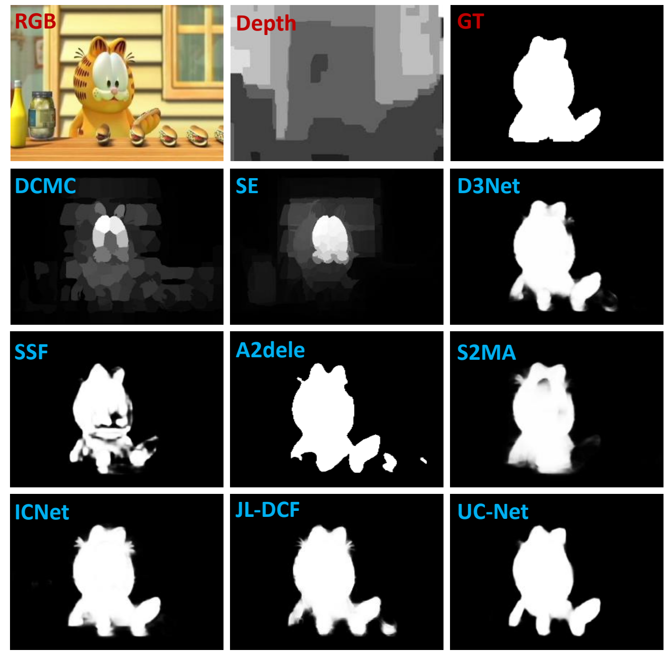

Fig. 1. RGB-D based salient object prediction on a sample image using two classic non-deep models (*i.e.*, DCMC [1] and SE [2]) and seven state-of-the-art deep models (*i.e.*, $\mathrm{D^3Net}$ [3], SSF [4], A2dele [5], $\mathrm{S^2MA}$ [6], ICNet [7], JL-DCF [8], and UC-Net [9]).

I. Introduction

Salient object detection (SOD) aims to locate the most visually prominent object(s) in a given scene [10]. SOD plays a key role in a range of real-world applications, such as stereo matching [11], image understanding [12], co-saliency detection [13], action recognition [14], video detection and segmentation [15]–[18], semantic segmentation [19], [20], medical image segmentation [21]–[23], object tracking [24], [25], person re-identification [26], [27], camouflaged object detection [28], image retrieval [29], *etc*. Although significant progress has been made in the SOD field over the past several years [30]–[36], [36]–[44], there is still room for improvement when faced with challenging factors, such as complicated background or different lighting conditions in the scenes. One way to overcome these challenges is to employ depth maps, which provide complementary spatial information for RGB images and have become easier to capture due to the large availability of depth sensors (*e.g.*, Microsoft Kinect).

Recently, RGB-D based SOD has gained increasing attention and various methods have been developed [3], [45]. Early RGB-D based SOD models tended to extract handcrafted features and then fuse RGB image and depth maps. For example, Lang *et al.* [46], the first work on RGB-D based SOD, utilized Gaussian mixture models to model the distribution of depth-induced saliency. Ciptadi *et al.* [47] extracted 3D layout and shape features from depth measurements. Besides, several methods [48], [49], [49], [50] measure depth contrast using the depth difference between different regions. In [51], a multi-contextual contrast model including local, global, and background contrast was developed to detect salient objects using depth maps. More importantly, however, this work also provided the first large-scale RGB-D dataset for SOD. Despite the effectiveness achieved by traditional methods using handcrafted features, they tend to suffer from a limited generalization ability for low-level features and lack the high-level reasoning required for complex scenes. To address these limitations, several deep learning-based RGB-D SOD methods [3] have been developed, showing improved performance. DF [52] was the first model to introduce deep learning technology into the RGB-D based SOD task. More recently, various deep learning-based models [6]–[9], [53]–[55] have focused on exploiting effective multi-modal correlations and multi-scale/level information to boost SOD performance. To more clearly describe the progress in the RGB-D based SOD field, we provide a brief chronology in Fig. 2.

In this paper, we provide a comprehensive survey on RGB-D based SOD, aiming to thoroughly cover various aspects of the models for this task and provide insightful discussions on the challenges and open directions for future work. We also

Corresponding author: Ding-Ping Fan (dengpingfan@mail.nankai.edu.cn).
T. Zhou, D.-P. Fan, J. Shen, and L. Shao are with Inception Institute of Artificial Intelligence, Abu Dhabi, UAE.
M.-M. Cheng is with CS, Nankai University, Tianjin 300350, China.

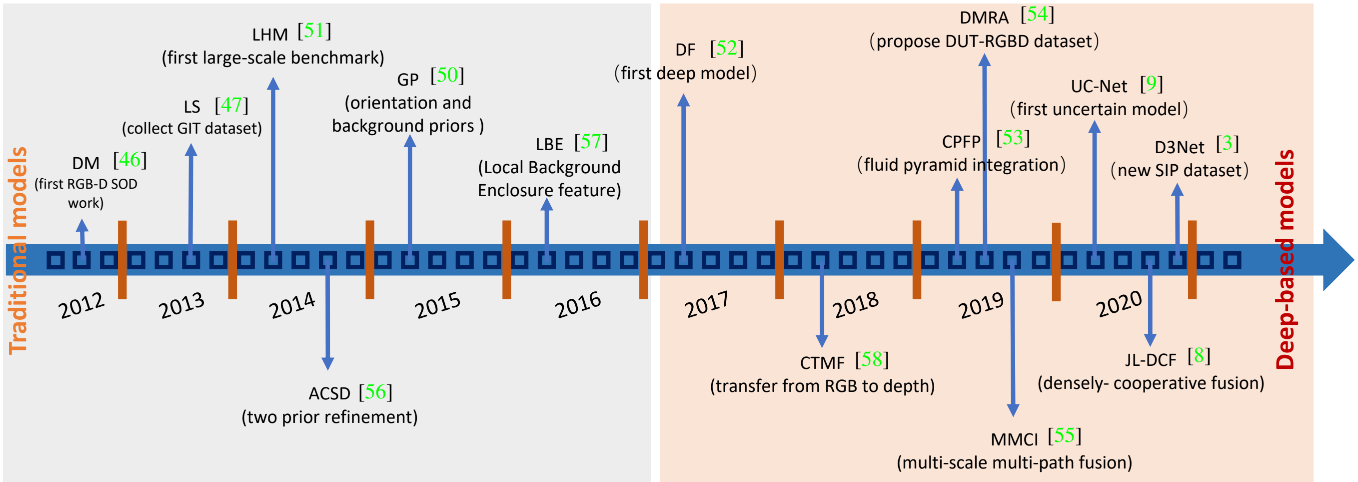

Fig. 2. A brief chronology of RGB-D based SOD. The first early RGB-D based SOD work was the DM [46] model, proposed in 2012. Deep learning techniques have been widely applied to RGB-D based SOD since 2017. More details can be found in § II.

review another related topic, *i.e.*, light field SOD, in which the light field can provide more information (including focal stack, all-focus images, and depth maps) to boost the performance of salient object detection. Further, we provide a comprehensive comparison to evaluate existing RGB-D based SOD models and discuss their main advantages.

A. Related Reviews and Surveys

There are several surveys that are closely related to salient object detection. For example, Borji *et al.* [59] provided a quantitative evaluation of 35 state-of-the-art non-deep saliency detection methods. Cong *et al.* [60] reviewed several different saliency detection models, including RGB-D based SOD, co-saliency detection, and video SOD. Zhang *et al.* [61] provided an overview of co-saliency detection and reviewed its history, and summarized several benchmark algorithms in this field. Han *et al.* [62] reviewed the recent progress in SOD, including models, benchmark datasets, and evaluation metrics, as well as discussed the underlying connection among general object detection, SOD, and category-specific object detection. Nguyen *et al.* [63] reviewed various works related to saliency applications and provided insightful discussions on the role of saliency in each. Borji *et al.* [64] provided a comprehensive review of recent progress in SOD and discussed some related works, including generic scene segmentation, saliency for fixation prediction, and object proposal generation. Fan *et al.* [10] provided a comprehensive evaluation of several state-of-the-art CNNs-based SOD models, and proposed a high quality SOD dataset, termed **SOC** (details can be found at: http://dpfan.net/socbenchmark/). Zhao *et al.* [65] reviewed various deep learning-based object detection models and algorithms in detail, as well as various specific tasks, including SOD works. Wang *et al.* [66] focused on reviewing deep learning-based SOD models. Different from previous SOD surveys, in this paper, we focus on reviewing the existing RGB-D based SOD models and benchmark datasets.

B. Contributions

Our main contributions are summarized as follows:

- We provide the first systematic review of RGB-D based SOD models from different perspectives. We summarize existing RGB-D SOD models into traditional or deep methods, fusion-wise methods, single-stream/multi-stream methods, and attention-aware methods.
- We review nine RGB-D datasets that are commonly used in this field, and provide details for each dataset. Moreover, we provide a comprehensive as well as an attribute-based evaluation of several representative RGB-D based SOD models.
- We supply the first collection and review of the related light field SOD models and benchmark datasets.
- We thoroughly investigate several challenges for RGB-D based SOD, and the relation between SOD and other topics, shedding light on potential directions for future research.

C. Organization

In § II, we review existing RGB-D based models in terms of different aspects. In § III, we summarize and provide details for current benchmark datasets for RGB-D salient object detection. In § IV, we conduct a comprehensive review of light field SOD models and benchmark datasets. In § V, we provide a comprehensive and attribute-based evaluation of several representative RGB-D based models. We then discuss challenges and open directions of this field in § VI. Finally, we conclude this paper in § VII.

II. RGB-D BASED SOD MODELS

Over the past few years, several RGB-D based SOD methods have been developed and obtained promising performance. These models are summarized in Tables I, II, III and IV. The complete benchmark can be found at http://dpfan.net/d3netbenchmark/. To review these RGB-D based SOD models in detail,we introduce them from different perspectives as follows. (1) **Traditional/deep models**: they are viewed from the perspective of feature extraction, that is using the manual features or deep features. It is convenient for follow-up researchers to grasp the historical development trends of RGB-D SOD models. (2) **Fusion-wise models**: it is critical to effectively fuse RGB and depth images in this task, thus we review different fusion strategies to understand their effectiveness. (3) **Single-stream/multi-stream models**: we consider this problem from the perspective of model parameters. Single stream can save parameters, but the final result may not be optimal, and multiple streams may require more parameters. Thus, it is helpful to understand the balance between the amount of calculation and accuracy of different models. (4) **Attention-aware models**: attention mechanisms have widely been applied in various visual tasks including SOD. We review related works on RGB-D SOD to analyze how do different models use attention. Thus, it is an alternative to design attention modules for future works.

A. Traditional/Deep Models

Traditional Models. With depth cues, several useful attributes, such as boundary cues, shape attributes, surface normals, etc., can be explored to boost the identification of salient objects in complex scenes. Over the past several years, many traditional RGB-D models based on handcrafted features have been developed [1], [2], [47]–[51], [56], [57], [69]–[71], [75], [82]–[84], [95]. For example, the early work [47] focused on modeling the interaction between layout and shape features generated from the RGB image and depth map. Besides, the representative work [51] developed a novel multi-stage RGB-D model, and constructed the first large-scale RGB-D benchmark dataset, termed NLPR.

Deep Models. However, the above-mentioned methods suffer from unsatisfactory SOD performance due to the limited expression ability of handcrafted features. To address this, several studies have turned to deep neural networks (DNNs) to fuse RGB-D data [4], [5], [7]–[9], [52]–[55], [83], [93], [94], [96]–[108]. These models can learn high-level representations to explore complex correlations across RGB images and depth cues for improving SOD performance. We review some representative works in detail as follows.

- **DF** [52] develops a novel convolutional neural network (CNN) to integrate different low-level saliency cues into hierarchical features, for effectively locating salient regions in RGB-D images. This was the first CNN-based model for the RGB-D SOD task. However, it utilizes a shallow architecture to learn the saliency map.
- **PCF** [92] presents a complementarity-aware fusion module to integrate cross-modal and cross-level feature representations. It can effectively exploit complementary information by explicitly using cross-modal/level connections and modal/level-wise supervision to decrease fusion ambiguity.
- **CTMF** [58] employs a computational model to identify salient objects from RGB-D scenes, utilizing CNNs to learn high-level representations for RGB images and depth cues, while simultaneously exploiting the complementary relationships and joint representation. Besides, this model transfers the structure of the model from the source domain (*i.e.*, RGB images) to be applicable to the target domain (*i.e.*, depth maps).
- **CPFP** [53] proposes a contrast-enhanced network to produce an enhanced map, and presents a fluid pyramid integration module to effectively fuse cross-modal information in a hierarchical manner. Besides, considering the fact that depth cues tend to suffer from noise, a feature-enhanced module is proposed to learn an enhanced depth cue for boosting the SOD performance. It is worth noting that this is an effective solution.
- **UC-Net** [9] proposes a probabilistic RGB-D based SOD network via conditional variational autoencoders (VAEs) to model human annotation uncertainty. It generates multiple saliency maps for each input image by sampling in the learned latent space. This was the first work to investigate uncertainty in RGB-D based SOD, and was inspired by the data labeling process. This method leverages the diverse saliency maps to improve the final SOD performance.

B. Fusion-wise Models

For RGB-D based SOD models, it is important to effectively fuse RGB images and depth maps. The existing fusion strategies can be grouped into three categories, including 1) early fusion, 2) multi-scale fusion, and 3) late fusion. We provide details for each fusion strategy as follows.

Early Fusion. Early fusion-based methods can follow one of two veins: 1) RGB images and depth maps are directly integrated to form a four-channel input [50], [51], [87], [87], [96]. This is denoted as "input fusion" (shown in Fig. 3); 2) RGB and depth images are first fed into each independent network and their low-level representations are combined as joint representations, which are then fed into a subsequent network for further saliency map prediction [52]. This is denoted as "early feature fusion" (shown in Fig. 3).

Late Fusion. Late fusion-based methods can also be further divided into two families: 1) Two parallel network streams are adopted to learn high-level features for RGB and depth data, respectively, which are concatenated and then used for generating the final saliency prediction [48], [58], [102]. This is denoted as "later feature fusion" (shown in Fig. 3). 2) Two parallel network streams are used to obtain the independent saliency maps for RGB images and depth cues, and then the two saliency maps are concatenated to obtain a final prediction map [115]. This is denoted as "late result fusion" (shown in Fig. 3).

Multi-scale Fusion. To effectively explore the correlations between RGB images and depth maps, several methods propose a multi-scale fusion strategy [7], [8], [55], [116], [120], [123], [124], [129]. These models can be divided into two categories. The first category learn the cross-modal interactions and then fuse them into a feature learning network. For example, Chen *et al.* [55] developed a multi-scale multi-path fusion network to integrate RGB images and depth maps, with a cross-modal interaction (termed MMCI) module. This method introduces cross-modal interactions into multiple layers, which can empower additional gradients for enhancing the learning of the depth stream, as well as enable complementarity across low-level and high-level representations to be explored. The second category fuse the features from RGB images and depth

TABLE I
SUMMARY OF RGB-D BASED SOD METHODS (PUBLISHED FROM 2012 TO 2016).

#	Year	Method	Pub.	Training Set	Backbone	Description
1	2012	DM [46]	ECCV	Without	Without	Models the correlation between saliency and depth by approximating the joint density using Gaussian mixture models
2	2012	RCM [67]	ICCSE	Without	Without	Develops a region contrast based SOD model with depth cues
3	2013	LS [47]	BMVC	Without	Without	Extends the dissimilarity framework to model the joint interaction between depth cues and RGB images
4	2013	RC [48]	BMVC	Withoutt	Without	Derives RGB-D saliency by formulating a 3D saliency model based on the region contrast of the scene and fuses it using SVM
5	2013	SOS [68]	NEURO	Without	Without	Incorporates depth cues for salient object segmentation by suppressing background regions
6	2014	SRDS [69]	ICDSP	Without	Without	Integrates depth and depth weighted color contrast with spatial compactness of color distribution
7	2014	LHM [51]	ECCV	Without	Without	Uses a multi-stage RGB-D algorithm to combine both depth and appearance cues to segment salient objects
8	2014	DESM [49]	ICIMCS	Without	Without	Combines three saliency cues: color contrast, spatial bias, and depth contrast
9	2014	ACSD [56]	ICIP	Without	Without	Measures a point's saliency by how much it stands out from the surroundings, and has two priors (regions nearer to viewers are more salient and salient objects tend to be located at the center)
10	2015	GP [50]	CVPRW	Without	Without	Explores orientation and background priors for detecting salient objects, and uses PageRank and MRFs to optimize the saliency maps
11	2015	SFP [70]	ICIMCS	Without	Without	Develops a RGB-D based SOD approach using saliency fusion and propagation
12	2015	DIC [71]	TVC	Without	Without	Fuses the saliency maps from color and depth to generate a noise-free salient patch, and utilizes random walk algorithm to infer the object boundary
13	2015	SRD [72]	ICRA	Without	Without	Designs a graph-based segmentation to identify homogeneous regions using color and depth cues
14	2015	MGMR [73]	ICIP	Without	Without	Designs a mutual guided manifold ranking strategy to achieve SOD
15	2015	SF [74]	CAC	Without	Without	Proposes to automatically select discriminative features using decision trees for better performance
16	2016	PRC [75]	ACCESS	Without	Without	Saliency fusion and progressive region classification are used to optimize depth-aware saliency models
17	2016	LBE [57]	CVPR	Without	Without	Uses a local background enclosure to capture the spread of angular directions
18	2016	SE [2]	ICME	Without	Without	Utilizes cellular automata to propagate the initial saliency map and then generate the final saliency prediction result
19	2016	DCMC [1]	SPL	Without	Without	Develops a new measure to evaluate the reliability of depth maps for reducing the influence of poor-quality depth maps on saliency detection.
20	2016	BF [76]	ICPR	Without	Without	Fuses contrasting features from RGB and depth images with a Bayesian framework
21	2016	DCI [77]	ICASSP	Without	Without	Adopts the original depth map to subtract the fitted surface for generating a contrast increased map
22	2016	DSF [78]	ICASSP	Without	Without	Develops a multi-stage depth-aware saliency model for SOD
23	2016	GM [79]	ACCV	Without	Without	Combines color and depth-based contrast features using a generative mixture model

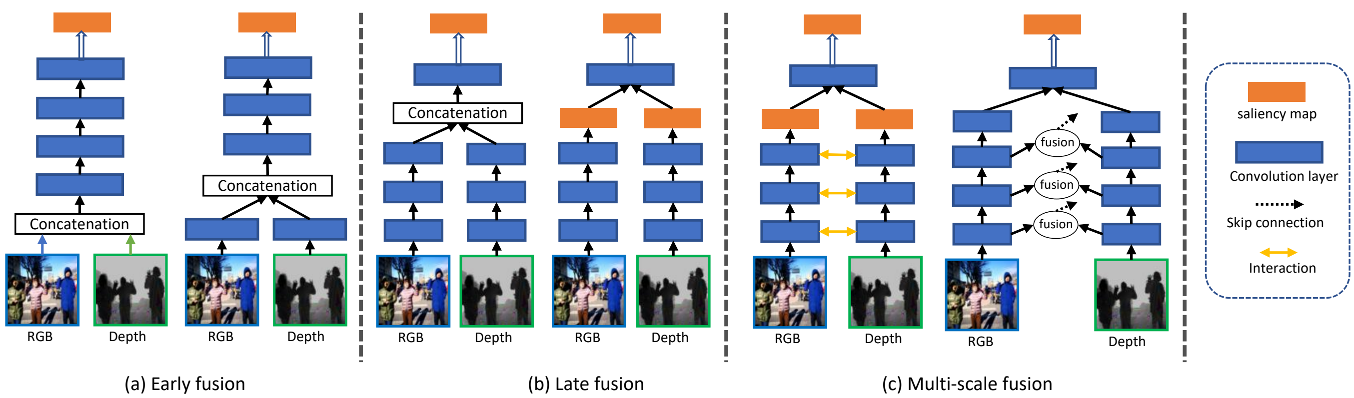

Fig. 3. Comparison of three fusion strategies that explore the correlation between RGB images and depth maps for RGB-D based SOD. These include: 1) Early fusion; 2) Late fusion; 3) Multi-scale fusion.

maps in different layers and then integrate them into a decoder network (*e.g.*, skip connection) to produce the final saliency detection map (as shown in Fig. 3). Some representative works are briefly discussed as follows.

- **ICNet** [7] proposes an information conversion module to convert high-level features in an interactive manner. In this model, a cross-modal depth-weighted combination (CDC) block is introduced to enhance RGB features with depth features at different levels.

- **DPANet** [116] uses a gated multi-modality attention (GMA) module to exploit long-range dependencies. The GMA module can extract the most discriminative features by utilizing a spatial attention mechanism. Besides, this model controls the fusion rate of the cross-modal information using a gate function, which can reduce some effects brought by the unreliable depth cues.

- **BiANet** [120] employs a multi-scale bilateral attention module (MBAM) to capture better global information in multiple layers.

- **JL-DCF** [8] treats a depth image as a special case of a color image and employs a shared CNN for both RGB and depth feature extraction. It also proposes a densely-cooperative fusion strategy to effectively combine the learned features from different modalities.

TABLE II
SUMMARY OF RGB-D BASED SOD METHODS (PUBLISHED FROM 2017 TO 2018).

#	Year	Method	Pub.	Training Set	Backbone	Description
24	2017	HOSO [80]	DICTA	Without	Without	Combines surface orientation distribution contrast with color and depth contrast
25	2017	M^3Net [81]	IROS	NLPR(0.65K), NJUD(1.4K)	VGG-16	Designs a multi-path multi-modal fusion strategy to integrate RGB and depth images in a task-motivated and adaptive way
26	2017	MFLN [82]	ICCVS	NLPR(0.65K), NJUD(1.4K)	AlexNet	Leverages a CNN to learn high-level representations for depth maps, and uses a multi-modal fusion network to integrate RGB and depth representations for RGB-D based SOD
27	2017	BED [83]	ICCVW	NLPR(0.6K), NJUD(1.2K)	GoogleNet	Uses a CNN to integrate top-down and bottom-up information for RGB-D based SOD, and uses a mid-level feature representation to capture background enclosure
28	2017	CDCP [84]	ICCVW	Without	Without	Proposes a novel RGB-D SOD algorithm using a center dark channel prior to boost performance
29	2017	TPF [85]	ICCVW	Without	Without	Leverages stereopsis to generate optical flow, which can provide an additional cue (depth cue) for producing the final detection result
30	2017	MFF [86]	SPL	Without	Without	Uses a multistage fusion framework to integrate multiple visual priors from the RGB image and depth cue for SOD
31	2017	MDSF [87]	TIP	NLPR(0.5K), NJUD(1.5K)	Without	Proposes a RGB-D SOD framework via a multi-scale discriminative saliency fusion strategy, and utilizes bootstrap learning to achieve the SOD task
32	2017	DF [52]	TIP	NLPR(0.75K), NJUD(1.0K)	Without	Feeds RGB and depth features into a CNN architecture to derive the saliency confidence value, and uses Laplacian propagation to produce the final detection result
33	2017	MCLP [88]	TCYB	Without	Without	Utilizes the additional depth maps and employs the existing RGB saliency map as an initialization using a refinement-cycle model to obtain the final co-saliency map
34	2018	ISC [89]	SIVP	Without	Without	Fuses salient features using both bottom-up and top-down saliency cues
35	2018	HSCS [90]	TMM	Without	Without	Utilizes a hierarchical sparsity reconstruction and energy function refinement for RGB-D based co-saliency detection
36	2018	ICS [91]	TIP	Without	Without	Exploits the constraint correlation among multiple images and introduces depth maps into the co-saliency model
37	2018	CTMF [58]	TCYB	NLPR(0.65K), NJUD(1.4K)	VGG-16	Transfers the structure of the deep color network to be applicable for the depth modality and fuses both modalities to produce the final saliency map
38	2018	PCF [92]	CVPR	NLPR(0.65K), NJUD(1.4K)	VGG-16	Designs the first multi-scale fusion architecture and a novel complementarity-aware fusion module to fuse both cross-modal and cross-level features
39	2018	SCDL [93]	ICDSP	NLPR(0.75K), NJUD(1.0K)	VGG-16	Designs a new loss function to increase the spatial coherence of salient objects
40	2018	ACCF [94]	IROS	NLPR(0.65K), NJUD(1.4K)	VGGNet	Adaptively selects complementary features from different modalities at each level, and then performs more informative cross-modal cross-level combinations
41	2018	CDB [95]	NEURO	Without	Without	Utilizes a contrast prior and depth-guided-background prior to construct a 3D stereoscopic saliency model

• **BBS-Net** [129] uses a bifurcated backbone strategy (BBS) to split the multi-level feature representations into teacher and student features, and develops a depth-enhanced module (DEM) to explore informative parts in depth maps from the spatial and channel views.

C. Single-stream/Multi-stream Models

Single-stream Models. Several RGB-D based SOD works [52], [53], [83], [87], [93], [96], [97] focus on a single-stream architecture to achieve saliency prediction. These models often fuse RGB images and depth information in the input channel or feature learning part. For example, MDSF [87] employs a multi-scale discriminative saliency fusion framework as the SOD model, in which four types of features in three levels are computed and then fused to obtain the final saliency map. BED [83] utilizes a CNN architecture to integrate bottom-up and top-down information for SOD, which also incorporates multiple features, including background enclosure distribution (BED) and low level depth maps (*e.g.*, depth histogram distance and depth contrast) to boost the SOD performance. PDNet [97] extracts depth-based features using a subsidiary network, which makes full use of depth information to assist the main-stream network.

Multi-stream Models. Two-stream models [54], [102], [103] consist of two independent branches that process RGB images and depth cues, respectively, and often generate different high-level features or saliency maps and then incorporate them in the middle stage or end of the two streams. It is worth noting that most recent deep learning-based models [5], [7], [45], [55], [92], [100], [104], [106], [116], [118] utilize this two-stream architecture with several models capturing the correlations between RGB images and depth cues across multiple layers. Moreover, some models utilize a multi-stream structure [3], [99] and then design different fusion modules to effectively fuse RGB and depth information in order to exploit their correlations.

D. Attention-aware Models

Existing RGB-D based SOD methods often treat all regions equally using the extracted features equally, while ignoring the fact that different regions can have different contributions to the final prediction map. These methods are easily affected by cluttered backgrounds. In addition, some methods either regard the RGB images and depth maps as having the same status or overly rely on depth information. This prevents them from considering the importance of different domains (RGB images or depth cues). To overcome this, several methods introduce attention mechanisms to weight the importance of different regions or domains.

• **ASIF-Net** [106] captures complementary information from RGB images and depth cues using an interweaved fusion, and weights the saliency regions through a deeply supervised attention mechanism.

• **AttNet** [103] introduces attention maps for differentiating between salient objects and background regions to reduce the negative influence of some low-quality depth cues.

TABLE III
SUMMARY OF RGB-D BASED SOD MODELS PUBLISHED IN 2019 AND 2020

No.	Year	Method	Pub.	Training Set	Backbone	Description
42	2019	SSRC [96]	NEURO	NLPR(0.65K), NJUD(1.4K)	VGG-16	Uses a single-stream recurrent convolutional neural network with a four-channel input and DRCNN subnetwork
43	2019	MLF [109]	SPL	NJUD(1.588K)	VGG-16	Designs a salient object-aware data augmentation method to expand the training set
44	2019	TSRN [110]	ICIP	NJUD(1.387K)	VGG-16	Designs a fusion refinement module to integrate output features from different modalities and resolutions
45	2019	DIL [111]	MTAP	NLPR(0.5K), NJUD(0.5K)	Without	Designs a consistency integration strategy to generate an image pre-segmentation result that is consistent with the depth distribution
46	2019	CAFM [112]	TSMC	NUS [46], NCTU [113]	VGG-16	Utilizes a content-aware fusion module to integrate global and local information
47	2019	PDNet [97]	ICME	NLPR(0.5K), NJUD(1.5K)	VGG-16	Adopts a prior-model guided master network to process RGB information, which is pre-trained on the conventional RGB dataset to overcome the limited size
48	2019	MMCI [55]	PR	NLPR(0.65K), NJUD(1.4K)	VGG-16	Improves the traditional two-stream architecture by diversifying the multi-modal fusion paths and introducing cross-modal interactions in multiple layers
49	2019	TANet [99]	TIP	NLPR(0.65K), NJUD(1.4K)	VGG-16	Uses a three-stream multi-modal fusion framework to explore cross-modal complementarity in both the bottom-up and top-down processes
50	2019	DCMF [100]	TCYB	NLPR(0.65K), NJUD(1.4K)	VGG-16	Formulates a CNN-based cross-modal transfer learning problem for depth-induced SOD, and uses a dense cross-level feedback strategy to exploit cross-level interactions
51	2019	DGT [101]	TCYB	Without	Without	Exploits depth cues and provides a general transformation model from RGB saliency to RGB-D saliency
52	2019	LSF [45]	arXiv	NLPR(0.65K), NJUD(1.4K)	VGG	Designs an RGB-D system with three key components, including modality-specific representation learning, complementary information selection, and cross-modal complements fusion
53	2019	AFNet [102]	ACCESS	NLPR(0.65K), NJUD(1.4K)	VGG-16	Learns a switch map that is used to adaptively fuse the predicted saliency maps from the RGB and depth modality
54	2019	EPM [114]	ACCESS	Without	Without	Develops an effective propagation mechanism for RGB-D co-saliency detection
55	2019	CPFP [53]	CVPR	NLPR(0.65K), NJUD(1.4K)	VGG-16	Uses a contrast-enhanced network to obtain the one-channel enhanced map, and designs a fluid pyramid integration module to fuse cross-modal cross-level features in a pyramid style
56	2019	DMRA [54]	ICCV	NLPR(0.7K), NJUD(1.485K)	VGG-19	Designs a depth-induced multiscale recurrent attention network for SOD, including a depth refinement block and a recurrent attention module
57	2019	DSD [115]	JVCIR	NLPR(0.5K), NJUD(1.5K)	VGG-16	Uses a saliency fusion network to adaptively fuse both the color and depth saliency maps
58	2020	DPANet [116]	arXiv	NLPR(0.65K), NJUD(1.4K), DUT(0.8K)	ResNet-50	Uses a saliency-orientated depth perception module to evaluate the potentiality of depth maps and reduce effects of contamination
59	2020	SSDP [117]	arXiv	NLPR(0.7K), NJUD(1.485K), DUT(0.8K)	VGG-19	Makes use of existing labeled RGB saliency datasets together with unlabeled RGB-D data to boost SOD performance
60	2020	AttNet [103]	IVC	NLPR(0.65K), NJUD(1.4K)	VGG-16	Deploys attention maps to boost the salient objects' location and pays more attention to the appearance information
61	2020	— [104]	NEURO	NLPR(0.65K), NJUD(1.4K)	VGG-16	Uses an adaptive gated fusion module via a GAN to obtain a better fused saliency map from RGB images and depth cues
62	2020	CoCNN [105]	PR	STERE, NJUD	VGG-16	Fuses color and disparity features from low to high layers in a unified deep model
63	2020	cmSalGAN [118]	TMM	NLPR(0.65K), NJUD(1.4K)	ResNet-50	Aims to learn an optimal view-invariant and consistent pixel-level representation for both RGB and depth images using an adversarial learning framework
64	2020	PGHF [119]	ACCESS	NLPR(0.65K), NJUD(1.4K)	VGG-16	Leverages powerful representations learned from large-scale RGB datasets to boost the model ability

• **TANet** [99] formulates a multi-modal fusion framework using RGB images and depth maps from the bottom-up and top-down views. It then introduces a channel-wise attention module to effectively fuse the complementary information from different modalities and levels.

E. Open-source Implementations

We summarize the open-source implementations of RGB-D based SOD models reviewed in this survey. The implementations and hyperlinks of the source codes of these models are provided in Tab V. More source codes will be updated at: https://github.com/taozh2017/RGBD-SODsurvey.

III. RGB-D DATASETS

With the rapid development of RGB-D based SOD, various datasets have been constructed over the past several years. Tab VI summarizes nine popular RGB-D datasets, and Fig. 4 shows examples of images (including RGB images, depth maps, and annotations) from these datasets. Moreover, we provide the details for each dataset as follows.

• **STERE** [138]. The authors first collected 1,250 stereoscopic images from Flickr [1], NVIDIA 3D Vision Live [2], and Stereoscopic Image Gallery [3]. The most salient objects in each image were annotated by three users. All annotated images were then sorted based on the overlaping salient regions and the top 1,000 images were selected to construct the final dataset. This is the first collection of stereoscopic images in this field.

• **GIT** [47] consists of 80 color and depth images, which were collected using a mobile-manipulator robot in a real-world home environment. Moreover, each image is annotated based on the pixel-level segmentation of the objects.

• **DES** [49] consists of 135 indoor RGB-D images, which were taken by Kinect with a resolution of 640×640. When

[1] http://www.flickr.com/
[2] http://photos.3dvisionlive.com/
[3] http://www.stereophotography.com/

TABLE IV
SUMMARY OF RGB-D BASED SOD MODELS PUBLISHED IN 2020.

No.	Year	Method	Pub.	Training Set	Backbone	Description
65	2020	BiANet [120]	TIP	NLPR(0.7K), NJUD(1.485K)	VGG-16	Uses a bilateral attention module (BAM) to explore rich foreground and background information from depth maps
66	2020	ASIF-Net [106]	TCYB	NLPR(0.65K), NJUD(1.4K)	VGG-16	Integrates the attention steered complementarity from RGB-D images and introduces a global semantic constraint using adversarial learning
67	2020	Triple-Net [107]	SPL	Triple-Net	ResNe-18	Uses a triple-complementary network for RGB-D based SOD
68	2020	ICNet [7]	TIP	Triple-Net	VGG-16	Uses a novel information conversion module to fuse high-level RGB and depth features in an interactive and adaptive way
69	2020	SDF [108]	TIP	NLPR,NJUD, DEC,LFSD(1.5K)	VGG-16	Proposes a exemplar-driven method to estimate relatively trustworthy depth maps, and uses a selective deep saliency fusion network to effectively integrate RGB images, original depths, and newly estimated depths
70	2020	GFNet [121]	SPL	NLPR(0.8K), NJUD(1.588K)	Res2Net	Designs a gate fusion block to regularize feature fusion
71	2020	RGBS [122]	MTAP	NLPR(0.65K), NJUD(1.4K)	VGG-16	Utilizes a GAN to generate the saliency map
72	2020	D^3Net [3]	TNNLS	NLPR(0.7K), NJUD(1.485K)	VGG-16	Uses a depth depurator unit (DDU) and a three-stream feature learning module to employ low-quality depth cue filtering and cross-modal feature learning, respectively
73	2020	JL-DCF [8]	CVPR	NLPR(0.7K), NJUD(1.5K)	VGG-16, ResNet-101	Uses a joint learning strategy and a densely-cooperative fusion module to achieve better SOD performance
74	2020	A2dele [5]	CVPR	NLPR(0.7K), NJUD(1.485K)	VGG-16	Employs a depth distiller to explore ways of using network prediction and attention as two bridges to transfer depth knowledge to RGB images
75	2020	SSF [4]	CVPR	NLPR(0.7K), NJUD(1.485K), DUT(0.8K)	AGG-16	Designs a complimentary interaction module to select useful representations from the RGB and depth images and then integrate cross-modal features
76	2020	S^2MA [6]	CVPR	NLPR(0.65K), NJUD(1.4K)	VGG-16	Fuses multi-modal information via self-attention and each other's attention strategies, and reweights the mutual attention term to filter out unreliable information
77	2020	UC-Net [9]	CVPR	NLPR(0.7K), NJUD(1.5K)	VGG-16	Uses a probabilistic RGB-D saliency detection network via a conditional VAE to generate multiple saliency maps
78	2020	CMWNet [123]	ECCV	NLPR(0.65K), NJUD(1.4K)	VGG-16	Exploits feature interactions using three cross-modal cross-scale weighting modules to improve SOD performance
79	2020	HDFNet [124]	ECCV	NLPR(0.7K), NJUD(1.485K), DUT(0.8K)	VGG-16	Designs a hierarchical dynamic filtering network to effectively make use of cross-modal fusion information
80	2020	CAS-GNN [125]	ECCV	NLPR(0.65K), NJUD(1.4K)	VGG-16	Designs cascaded graph neural networks to exploit useful knowledge from RGB and depth images for building powerful feature embeddings
81	2020	CMMS [126]	ECCV	NLPR(0.7K), NJUD(1.485K)	VGG-16	Proposes a cross-modality feature modulation module to enhance feature representations and an adaptive feature selection module to gradually select saliency-related features
82	2020	DANet [127]	ECCV	NLPR(0.65K), NJUD(1.4K)	VGG-16, VGG-19	Develops a single-stream network combined with a depth-enhanced dual attention to achieve real-time SOD
83	2020	CoNet [128]	ECCV	NLPR(0.7K), NJUD(1.485K), DUT(0.8K)	ResNet	Develops a collaborative learning framework for RGB-D based SOD. Three collaborators (edge detection, coarse salient object detection and depth estimation) are utilized to jointly boost the performance
84	2020	BBS-Net [129]	ECCV	NLPR(0.65K), NJUD(1.4K)	VGG-16, VGG-19, ResNet-50	Uses a bifurcated backbone strategy to learn teacher and student features, and utilizes a depth-enhanced module to excavate informative parts of depth cues
85	2020	ATSA [130]	ECCV	NLPR(0.7K), NJUD(1.485K), DUT(0.8K)	VGG-19	Proposes an asymmetric two-stream architecture taking account of the inherent differences between RGB and depth data for SOD
86	2020	PGAR [131]	ECCV	NLPR(0.7K), NJUD(1.485K)	VGG-16	Propose a progressively guided alternate refinement network to produce a coarse initial prediction using a multi-scale residual block
87	2020	MCINet [132]	arXiv	NLPR(0.65K), NJUD(1.4K)	ResNet-50	Develops a novel multi-level cross-modal interaction network for RGB-D SOD
88	2020	DRLF [133]	TIP	NLPR(0.65K), NJUD(1.4K)	VGG-16	Develops a channel-wise fusion network to conduct multi-net and multi-level selective fusion for RGB-D SOD
89	2020	DQAM [134]	arXiv	NLPR(0.65K), NJUD(1.4K)	Without	Proposes a depth quality assessment solution to conduct "quality-aware" SOD for RGB-D images
90	2020	DQSD [135]	TIP	NLPR(0.65K), NJUD(1.4K)	VGG-19	Integrates a depth quality aware subnet into a bi-stream structure to assess the depth quality before conducting RGB-D fusion
91	2020	DASNet [136]	ACM MM	NLPR(0.7K), NJUD(1.5K)	ResNet-50	Proposes a new perspective of containing the depth constraints in the learning process rather than using depths as inputs
92	2020	DCMF [137]	TIP	NLPR(0.65K), NJUD(1.4K)	VGG-16, ResNet-50	Designs a disentangled cross-modal fusion network to expose structural and content representations from RGB and depth images

collecting this dataset, three users were asked to label the salient object in each image, and then the overlapping areas of the labeled object were regarded as the ground truth.

• **NLPR** [51] consists of 1,000 RGB images and their corresponding depth maps, which were obtained by a standard Microsoft Kinect. This dataset includes a series of outdoor and indoor locations, *e.g.*, offices, supermarkets, campuses, streets, and so on.

• **LFSD** [139] includes 100 light fields collected using a Lytro light field camera, and consists of 60 indoor and 40 outdoor scenes. To label this dataset, three individuals were asked to manually segment salient regions, and then the segmented results were deemed ground truth when the overlap of the three results was over 90%.

• **NJUD** [56] consists of 1,985 stereo image pairs, and these images were collected from the internet, 3D movies, and photographs that are taken by a Fuji W3 stereo camera.

• **SSD** [85] was constructed using three stereo movies and includes indoor and outdoor scenes. This dataset includes 80 samples, and each image has the size of 960×1080.

• **DUT-RGBD** [98] consists of 800 indoor and 400 outdoor

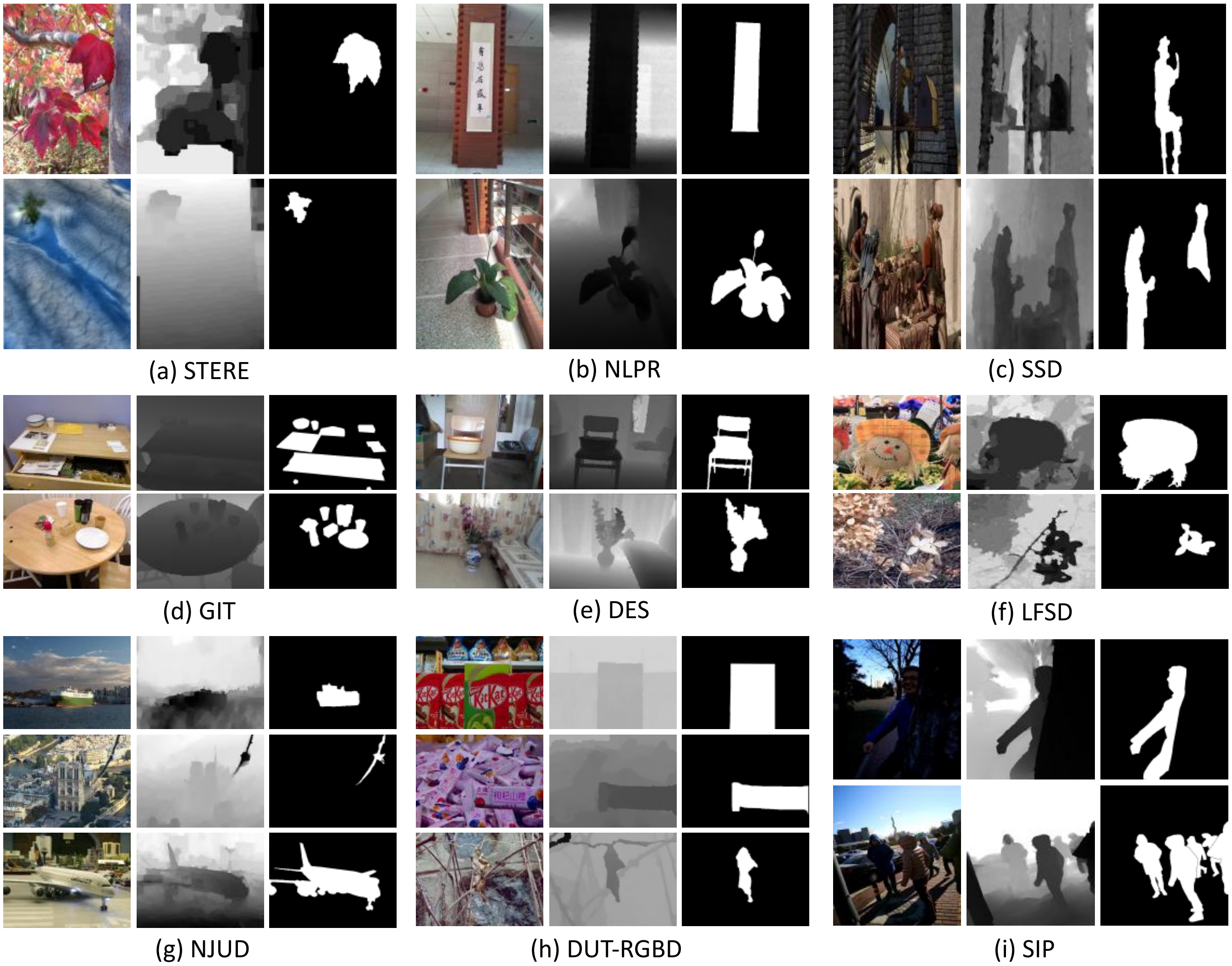

Fig. 4. Examples of images, depth maps and annotations in nine RGB-D dataset, including (a) STERE [138], (b) NLPR [51], (c) SSD [85], (d) GIT [47], (e) DES [49] , (f) LFSD [139], (g) NJUD [56], (h) DUT-RGBD [98], and (i) SIP [3]. In each dataset, the RGB image, depth map and annotation are shown from left to right.

scenes with their corresponding depth images. This dataset includes several challenging factors, *i.e.*, multiple or transparent objects, complex backgrounds, similar foregrounds and backgrounds, and low-intensity environments.

• **SIP** [3] consists of 929 annotated high-resolution images, with multiple salient persons in each image. In this dataset, depth maps were captured using a real smartphone (*i.e.*, Huawei Mate10). Besides, it is worth noting that this dataset covers diverse scenes, and various challenging factors, and is annotated with pixel-level ground truths.

Note that a detailed dataset statistics analysis (including center bias, size of objects, background objects, object boundary conditions, and number of salient objects) can be found in [3].

IV. Saliency Detection on Light Field

A. Light Field SOD Models

Existing works for SOD can be grouped into three categories according to the input data type, including RGB SOD, RGB-D SOD, and light field SOD [155]. We have already reviewed RGB-D based SOD models, in which depth maps provide layout information to improve SOD performance to some extent. However, inaccurate or low-quality depth maps often decrease the performance. To overcome this issue, light field SOD methods have been proposed to make use of rich information captured by the light field. Specifically, light field data contains an all-focus image, a focal stack, and a rough depth map [98]. A summary of related light field SOD works is provided in Tab VII. Further, to provide an in-depth understanding of these models, we also review them in more detail as follows.

Traditional/Deep Models. The classic models for light field SOD often use superpixel-level handcrafted features [98], [139], [141]–[146], [148], [154]. Early work [139], [146] showed that the unique refocusing capability of light fields can provide useful focusness, depth, and objectness cues. Thus, several SOD models using light field data were further proposed. For example, Zhang *et al.* [142] utilized a set of focal slices to compute the background prior, and then combined it with the location prior for SOD. Wang *et al.* [145] proposed a two-stage Bayesian fusion model to integrate

TABLE V
A SUMMARY OF RGB-D BASED SOD MODELS WITH OPEN-SOURCE IMPLEMENTATIONS.

Year	Model	Implementation	Code link
2014	LHM [51]	Matlab	https://sites.google.com/site/rgbdsaliency/code
	DESM [49]	Matlab	https://github.com/HzFu/DES_code
2015	GP [50]	Matlab	https://github.com/JianqiangRen/Global_Priors_RGBD_Saliency_Detection
2016	DCMC [1]	Matlab	https://github.com/rmcong/Code-for-DCMC-method
	LBE [57]	Matlab & C++	http://users.cecs.anu.edu.au/ u4673113/lbe.html
2017	BED [83]	Caffe	https://github.com/sshige/rgbd-saliency
	CDCP [84]	Matlab	https://github.com/ChunbiaoZhu/ACVR2017
	MDSF [87]	Matlab	https://github.com/ivpshu
	DF [52]	Matlab	https://pan.baidu.com/s/1Y-PqAjuH9xREBjfl7H45HA
2018	CTMF [58]	Caffe	https://github.com/haochen593/CTMF
	PCF [92]	Caffe	https://github.com/haochen593/PCA-Fuse_RGBD_CVPR18
	PDNet [97]	TensorFlow	https://github.com/cai199626/PDNet
2019	AFNet [102]	TensorFlow	https://github.com/Lucia-Ningning/Adaptive_Fusion_RGBD_Saliency_Detection
	CPFP [53]	Caffe	https://github.com/JXingZhao/ContrastPrior
	DMRA [54]	PyTorch	https://github.com/jiwei0921/DMRA
	DGT [101]	Matlab	https://github.com/rmcong/Code-for-DTM-Method
2020	ICNet [7]	Caffe	https://github.com/MathLee/ICNet-for-RGBD-SOD
	JL-DCF [8]	Pytorch, Caffe	https://github.com/kerenfu/JLDCF
	A2dele [5]	PyTorch	https://github.com/OIPLab-DUT/CVPR2020-A2dele
	SSF [4]	PyTorch	https://github.com/OIPLab-DUT/CVPR_SSF-RGBD
	ASIF-Net [106]	TensorFlow	https://github.com/Li-Chongyi/ASIF-Net
	S^{2}MA [6]	PyTorch	https://github.com/nnizhang/S2MA
	UC-Net [9]	PyTorch	https://github.com/JingZhang617/UCNet
	D^{3}Net [3]	PyTorch	https://github.com/DengPingFan/D3NetBenchmark
	CMWNet [123]	Caffe	https://github.com/MathLee/CMWNet
	HDFNet [124]	PyTorch	https://github.com/lartpang/HDFNet
	CMMS [126]	TensorFlow	https://github.com/Li-Chongyi/cmMS-ECCV20
	CAS-GNN [125]	PyTorch	https://github.com/LA30/Cas-Gnn
	DANet [127]	PyTorch	https://github.com/Xiaoqi-Zhao-DLUT/DANet-RGBD-Saliency
	CoNet [128]	PyTorch	https://github.com/jiwei0921/CoNet
	DASNet [136]	PyTorch	http://cvteam.net/projects/2020/DASNet/
	BBS-Net [129]	PyTorch	https://github.com/DengPingFan/BBS-Net
	ATSA [130]	PyTorch	https://github.com/sxfduter/ATSA
	PGAR [131]	PyTorch	https://github.com/ShuhanChen/PGAR_ECCV20
	FRDT [140]	PyTorch	https://github.com/jack-admiral/ACM-MM-FRDT

TABLE VI
STATISTICS OF NINE RGB-D BENCHMARK DATASETS IN TERMS OF YEAR (YEAR), PUBLICATION (PUB.), DATASET SIZE (SIZE), NUMBER OF OBJECTS IN THE IMAGES (#OBJ.), TYPE OF SCENE (TYPES), DEPTH SENSOR (SENSOR), AND RESOLUTION (RESOLUTION). SEE § III FOR MORE DETAILS ON EACH DATASET. THESE DATASETS CAN BE DOWNLOADED FROM OUR WEBSITE: HTTP://DPFAN.NET/D3NETBENCHMARK/.

#	Dataset	Year	Pub.	Size	#Obj.	Types	Sensor	Resolution
1	**STERE** [138]	2012	CVPR	1,000	∼One	Internet	Stereo camera+sift flow	$[251 \sim 1200] \times [222 \sim 900]$
2	**GIT** [47]	2013	BMVC	80	Multiple	Home environment	Microsoft Kinect	640×480
3	**DES** [49]	2014	ICIMCS	135	One	Indoor	Microsoft Kinect	640×480
4	**NLPR** [51]	2014	ECCV	1,000	Multiple	Indoor/outdoor	Microsoft Kinect	640×480, 480×640
5	**LFSD** [139]	2014	CVPR	100	One	Indoor/outdoor	Lytro Illum camera	360×360
6	**NJUD** [56]	2014	ICIP	1,985	∼One	Movie/internet/photo	FujiW3 camera+optical flow	$[231 \sim 1213] \times [274 \sim 828]$
7	**SSD** [85]	2017	ICCVW	80	Multiple	Movies	Sun's optical flow	960×1080
8	**DUT-RGBD** [98]	2019	ICCV	1,200	Multiple	Indoor/outdoor	–	400×600
9	**SIP** [3]	2020	TNNLS	929	Multiple	Person in the wild	Huawei Mate10	992×744

multiple contrasts for boosting SOD performance. Recently, several deep learning-based light field SOD models [150]–[153], [155], [156] have also been developed, obtaining remarkable performance. Besides, in [150], an attentive recurrent CNN was developed to fuse all focal slices, while the data diversity was increased using adversarial examples to enhance model robustness. Zhang *et al.* [152] developed a memory-oriented decoder for light field SOD, which fuses multi-level features in a top-down manner using high-level information to guide low-level feature selection. LFNet [155] employs a new integration module to fuse features from light field data according to their contributions and captures the spatial

TABLE VII
SUMMARY OF POPULAR LIGHT FIELD SOD METHODS.

No.	Year	Method	Pub.	Dataset	Description
1	2014	LFS [139]	CVPR	LFSD	The first light-field saliency detection algorithm employs objectness and focusness cues based on the refocusing capability of the light field
2	2015	WSC [141]	CVPR	LFSD	Uses a weighted sparse coding framework to learn a saliency/non-saliency dictionary
3	2015	DILF [142]	IJCAI	LFSD	Incorporates depth contrast to complement the disadvantage of color and conducts focusness-based background priors to boost the saliency detection performance
4	2016	RL [143]	ICASSP	LFSD	Utilizes the inherent structure information in light field images to improve saliency detection
5	2017	MA [144]	TOMM	HFUT, LFSD	Integrates multiple saliency cues extracted from light field images using a random-search-based weighting strategy
6	2017	BIF [145]	NPL	LFSD	Integrates color-based contrast, depth-induced contrast, focusness map of foreground slice, and background weighted depth contrast using a two-stage Bayesian integration framework
7	2017	LFS [146]	TPAMI	LFSD	An extension of [139]
8	2017	RLM [147]	ICIVC	LFSD	Utilizes the light field relative location measurement for SOD on light field images
9	2018	SGDC [148]	CVPR	LFSD	Designs a saliency-guided depth optimization framework for multi-layer light field displays
10	2018	DCA [149]	FiO	LFSD	Proposes a graph model depth-induced cellular automata to optimize saliency maps using light field data
11	2019	DLLF [150]	ICCV	DUTLF-FS, LFSD	Utilizes a recurrent attention network to fuse each slice from the focal stack to learn the most informative features
12	2019	DLSD [151]	IJCAI	DUTLF-MV	Formulates saliency detection into two subproblems, including 1) light field synthesis from a single view and 2) light-field-driven saliency detection
13	2019	Molf [152]	NIPS	UTLF-FS	Uses a memory-oriented decoder for light field SOD
14	2020	ERNet [153]	AAAI	DUTLF-FS, HFUT, LFSD	Uses an asymmetrical two-stream architecture to overcome computation-intensive and memory-intensive challenges in a high-dimensional light field data
15	2020	DCA [98]	TIP	LFSD	Presents a saliency detection framework on light fields based on the depth-induced cellular automata (DCA) model. It can enforce spatial consistency to optimize the inaccurate saliency map using the DCA model
16	2020	RDFD [154]	MTAP	LFSD	Defines a region-based depth feature descriptor extracted from the light field focal stack to facilitate low- and high-level cues for saliency detection
17	2020	LFNet [155]	TIP	DUTLF-FS, LFSD, HFUT	Utilizes a light field refinement module and a light field integration module to effectively integrate multiple cues (*i.e.*, focusness, depths and objectness) from light field images
18	2020	LFDCN [156]	TIP	Lytro Illum, LFSD, HFUT	Uses a deep convolutional network based on the modified DeepLab-v2 model to explore spatial and multi-view properties of light field images for saliency detection

structure of a scene to improve SOD performance.

Refinement based Models. Several refinement strategies have been used to enforce neighboring constraints or reduce the homogeneity of multiple modalities for SOD. For example, in [141], the saliency dictionary was refined using the estimated saliency map. The MA method [144] employs a two-stage saliency refinement strategy to produce the final prediction map, which enables adjacent superpixels to obtain similar saliency values. Besides, LFNet [155] presents an effective refinement module to reduce the homogeneity among different modalities as well refine their dissimilarities

B. Light Field Data for SOD

There are five representative datasets widely used in existing light field SOD models. We describe the details of each dataset as follows.

• **LFSD** [139] [4] consists of 100 light fields of different scenes with a 360 × 360 spatial resolution, captured using a Lytro light field camera. This dataset contains 60 indoor and 40 outdoor scenes, and most scenes consist of only one salient object. Besides, three individuals were asked to manually segment salient regions in each image, and then the ground truth was determined when all three segmentation results had an overlap of over 90%.

• **HFUT** [144] [5] consists of 255 light fields captured using a Lytro camera. In this dataset, most scenes contain multiple objects that appear within different locations and scales under complex background clutter.

• **DUTLF-FS** [150] [6] consists of 1,465 samples, 1,000 of which are used as the training set, while the remaining 465 images make up the test set. The resolution of each image is 600 × 400. This dataset contains several challenges, including lower contrast between salient objects and cluttered background, multiple disconnected salient objects, and dark or strong light conditions.

• **DUTLF-MV** [151] [7] consists of 1,580 samples, 1,100 of which are for training and the remaining is for testing. Images were captured by a Lytro Illum camera, and each light field consists of multi-view images and a corresponding ground truth.

• **Lytro Illum** [156] [8] consists of 640 light fields and the corresponding per-pixel ground-truth saliency maps. It includes several challenging factors, *e.g.*, inconsistent illumination conditions, and small salient objects existing in a similar or cluttered background.

V. MODEL EVALUATION AND ANALYSIS

A. Evaluation Metrics

We briefly review several popular metrics for SOD evaluation, *i.e.*, precision-recall (PR), F-measure [59], [157], mean absolute error (MAE) [158], structural measure (S-measure) [159], and enhanced-alignment measure (E-measure) [160].

[4]https://sites.duke.edu/nianyi/publication/saliency-detection-on-light-field/
[5]https://github.com/pencilzhang/HFUT-Lytro-dataset
[6]https://github.com/OIPLab-DUT/ICCV2019_Deeplightfield_Saliency
[7]https://github.com/OIPLab-DUT/IJCAI2019-Deep-Light-Field-Driven-Saliency-Detection-from-A-Single-View
[8]https://github.com/pencilzhang/MAC-light-field-saliency-net

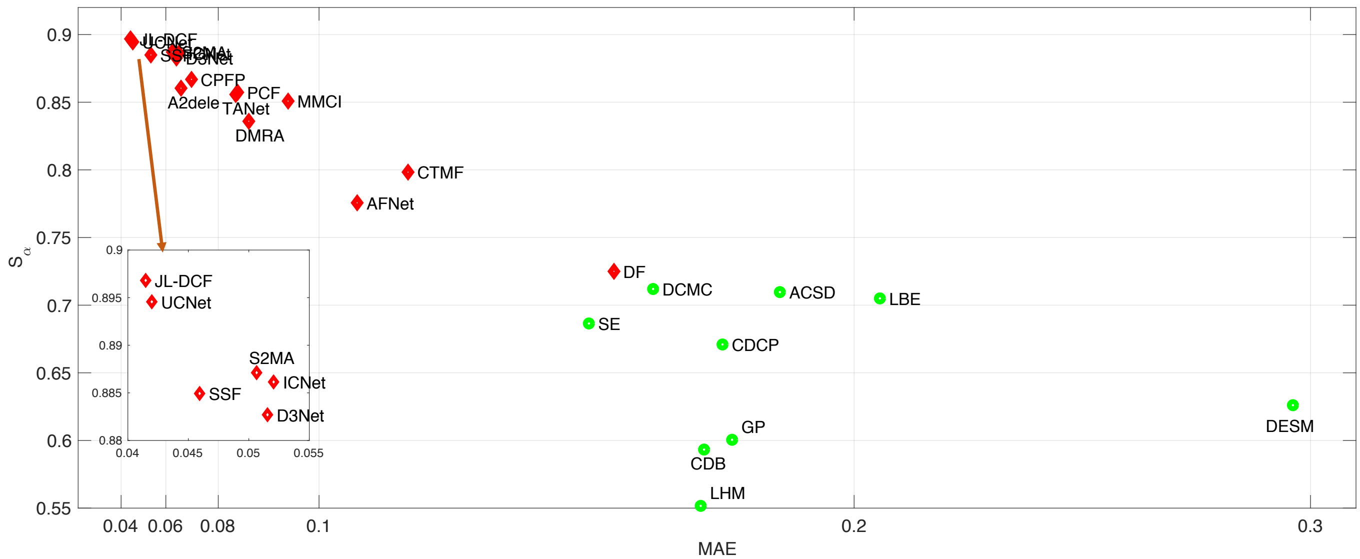

Fig. 5. A comprehensive evaluation for 24 representative RGB-D based SOD models, including LHM [51], ACSD [56], DESM [49], GP [50], LBE [57], DCMC [1], SE [2], CDCP [84], CDB [95], DF [52], PCF [92], CTMF [58], CPFP [53], TANet [99], AFNet [102], MMCI [55], DMRA [54], D^{3}Net [3], SSF [4], A2dele [5], S^{2}MA [6], ICNet [7], JL-DCF [8], and UC-Net [9]. We report the mean values of S_α and MAE across the five datasets (*i.e.*, STERE [138], NLPR [51], LFSD [139], DES [49], and SIP [3]) in each model. Note that better models are shown in the upper left corner (*i.e.*, with a larger S_α and smaller MAE). Here, red diamonds denote deep models and green circles denote traditional models.

• **PR**. Given a saliency map S, we can convert it to a binary mask M, and then compute the *precision* and *recall* by comparing M with ground-truth G:

$$Precision = \frac{|M \cap G|}{|M|},\ Recall = \frac{|M \cap G|}{|G|}. \quad (1)$$

A popular strategy is to partition the saliency map S using a set of thresholds (*i.e.*, it changes from 0 to 255). For each threshold, we first calculate a pair of recall and precision scores, and then combine them to obtain a PR curve that describes the performance of the model at the different thresholds.

• **F-measure** (F_β). To comprehensively consider both precision and recall, the F-measure is proposed by calculating the weighted harmonic mean:

$$F_\beta = \left(1+\beta^2\right)\frac{P * R}{\beta^2 P + R}, \quad (2)$$

where β^2 is set to 0.3 to emphasize the precision [157]. We use different fixed $[0, 255]$ thresholds to compute the F-measure metric. This yields a set of F-measure values for which we report the maximal or average F_β.

• **MAE**. This measures the average pixel-wise absolute error between a predicted saliency map S and a ground truth G for all pixels, which can be defined by

$$MAE = \frac{1}{W * H}\sum_{i=1}^{W}\sum_{i=1}^{H}\left|S_{i,j} - G_{i,j}\right|, \quad (3)$$

where W and H denote the width and height of the map, respectively. MAE values are normalized to [0,1].

• **S-measure** (S_α). To capture the importance of the structural information in an image, S_α [159] is used to assess the structural similarity between the regional perception (S_r) and object perception (S_o). Thus, S_α can be defined by

$$S_\alpha = \alpha * S_o + (1-\alpha) * S_r, \quad (4)$$

where $\alpha \in [0, 1]$ is a trade-off parameter. Here, we set $\alpha = 0.5$ as the default setting, as suggested by Fan *et al.* [159].

• **E-measure** (E_ϕ). E_ϕ [160] was proposed based on cognitive vision studies to capture image-level statistics and their local pixel matching information. Thus, E_ϕ can be defined by

$$E_\phi = \frac{1}{W * H}\sum_{i=1}^{W}\sum_{i=1}^{H}\phi_{FM}\left(i, j\right), \quad (5)$$

where ϕ_{FM} denotes the enhanced-alignment matrix [160].

B. Performance Comparison and Analysis

1) Overall Evaluation: To quantify the performance of different models, we conduct a comprehensive evaluation of 24 representative RGB-D based SOD models, including 1) nine traditional methods: LHM [51], ACSD [56], DESM [49], GP [50], LBE [57], DCMC [1], SE [2], CDCP [84], CDB [95]; and 2) fifteen deep learning-based methods: DF [52], PCF [92], CTMF [58], CPFP [53], TANet [99], AFNet [102], MMCI [55], DMRA [54], D^{3}Net [3], SSF [4], A2dele [5], S^{2}MA [6], ICNet [7], JL-DCF [8], and UC-Net [9]. We report the mean values of S_α and MAE across the five datasets (STERE [138], NLPR [51] , LFSD [139], DES [49], and SIP [3]) for each model in Fig. 5. It is worth noting that better models are shown in the upper left corner (*i.e.*, with a larger S_α and smaller MAE). From Fig. 5, we have following observations:

- **Traditional vs. Deep Models**. Compared with traditional RGB-D based SOD models, deep learning methods obtain significantly better performance. This confirms the powerful feature learning ability of deep networks.
- **Comparison of Deep Models**. Among the deep learning-based models, D^{3}Net [3], JL-DCF [8], UC-Net [9], SSF [4], ICNet [7], and S^{2}MA [6] obtain the best performance.

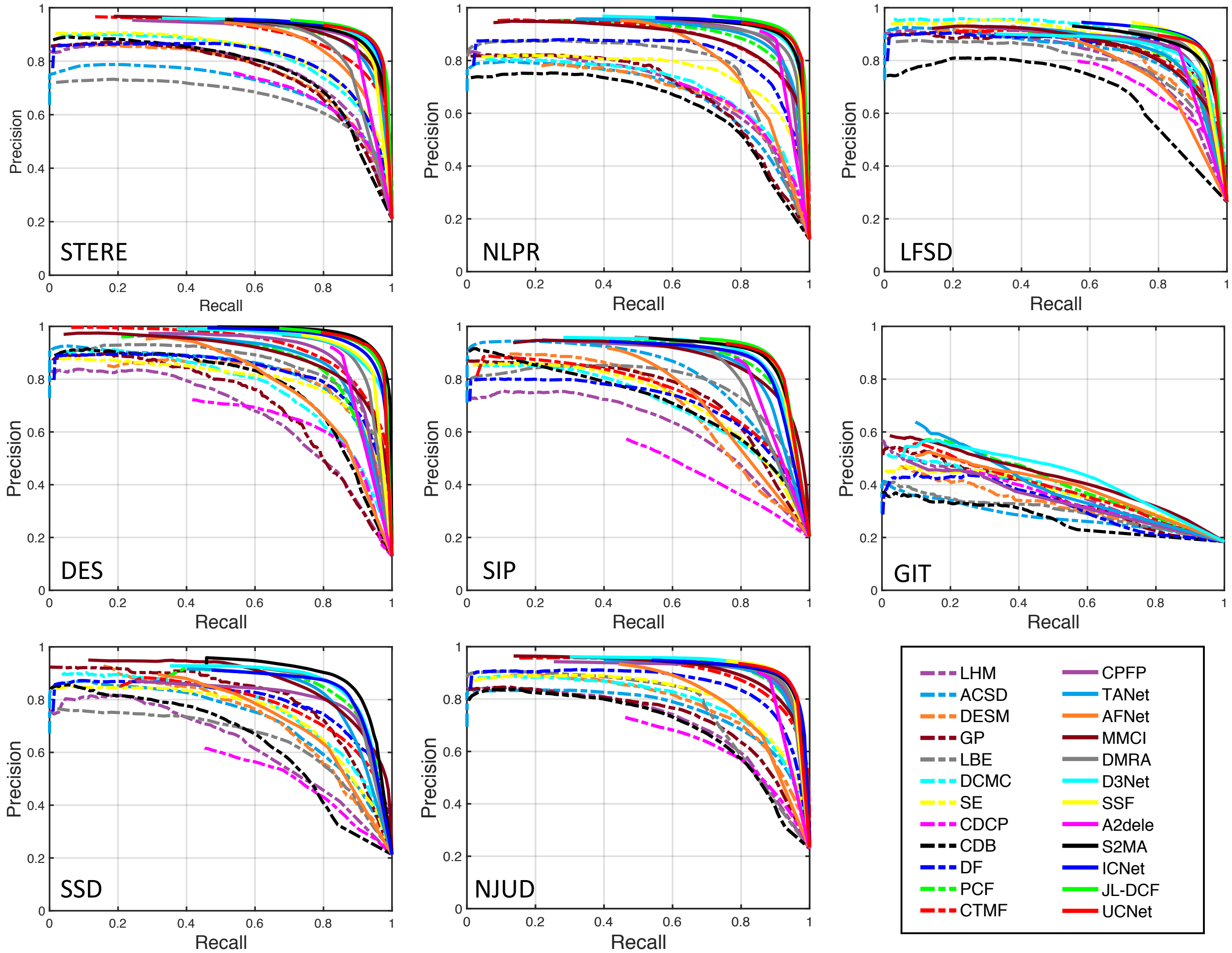

Fig. 6. PR curves for 24 RGB-D based models on the STERE [138], NLPR [51], LFSD [139], DES [49], SIP [3], GIT [47], SSD [85], and NJUD [56] datasets.

TABLE VIII

ATTRIBUTE-BASED STUDY *w.r.t.* SALIENT OBJECT SCALES. COMPARISON RESULTS FOR 24 REPRESENTATIVE RGB-D BASED SOD MODELS (9 TRADITIONAL MODELS AND 15 DEEP LEARNING-BASED MODELS) ARE PROVIDED IN TERMS OF MAE AND S_α. THE THREE BEST RESULTS ARE SHOWN IN RED, BLUE AND GREEN FONTS.

		Traditional models									Deep learning-based models														
	Scale	LHM [51]	ACSD [56]	DESM [49]	GP [50]	LBE [57]	DCMC [1]	SE [2]	CDCP [84]	CDB [95]	DF [52]	PCF [92]	CTMF [58]	CPFP [53]	TANet [99]	AFNet [102]	MMCI [55]	DMRA [54]	D^3Net [3]	SSF [4]	A2dele [5]	S^2MA [6]	ICNet [7]	JL-DCF [8]	UC-Net [9]
MAE	Small	.065	.149	.319	.098	.177	.108	.056	.128	.073	.087	.042	.065	.044	.041	.046	.051	.030	.033	.031	.032	.035	.036	.032	.034
	Medium	.178	.183	.287	.180	.210	.158	.150	.173	.179	.152	.068	.107	.055	.067	.095	.079	.069	.053	.045	.054	.052	.052	.041	.042
	Large	.403	.311	.310	.377	.261	.305	.364	.308	.385	.310	.112	.183	.093	.118	.213	.130	.181	.102	.105	.114	.088	.104	.085	.072
	Overall	.166	.184	.296	.173	.206	.156	.142	.171	.167	.147	.065	.102	.055	.065	.091	.076	.067	.052	.046	.053	.051	.052	.041	.042
S_α	Small	.624	.668	.517	.650	.645	.700	.775	.661	.666	.745	.847	.789	.840	.846	.792	.832	.860	.879	.876	.859	.877	.882	.881	.883
	Medium	.543	.732	.658	.598	.723	.727	.676	.683	.585	.730	.863	.805	.877	.862	.779	.859	.838	.888	.893	.865	.893	.892	.906	.901
	Large	.386	.630	.686	.450	.731	.604	.479	.586	.424	.597	.838	.761	.855	.827	.682	.830	.734	.846	.837	.815	.863	.845	.859	.876
	Overall	.552	.710	.626	.601	.705	.712	.686	.671	.593	.725	.857	.798	.867	.856	.776	.851	.836	.883	.885	.860	.887	.886	.897	.895

Moreover, Fig. 6 and Fig. 7 show the PR and F-measure curves for the 24 representative RGB-D based SOD models on eight datasets (*i.e.*, STERE [138], NLPR [51], LFSD [139], DES [49], SIP [3], GIT [47], SSD [85] , and NJUD [56]). Note that there are 1000, 300, 100, 135, 929, 80, and 80 test samples for NLPR, LFSD, DES, SIP, GIT, and SSD, respectively. For the NJUD [56] dataset, there are 485 test images for CPFP [53], S^2MA [6], ICNet [7], JL-DCF [8], and UC-Net [9], while 498 testing images for all other models.

To understand the top six models in depth, we discuss their

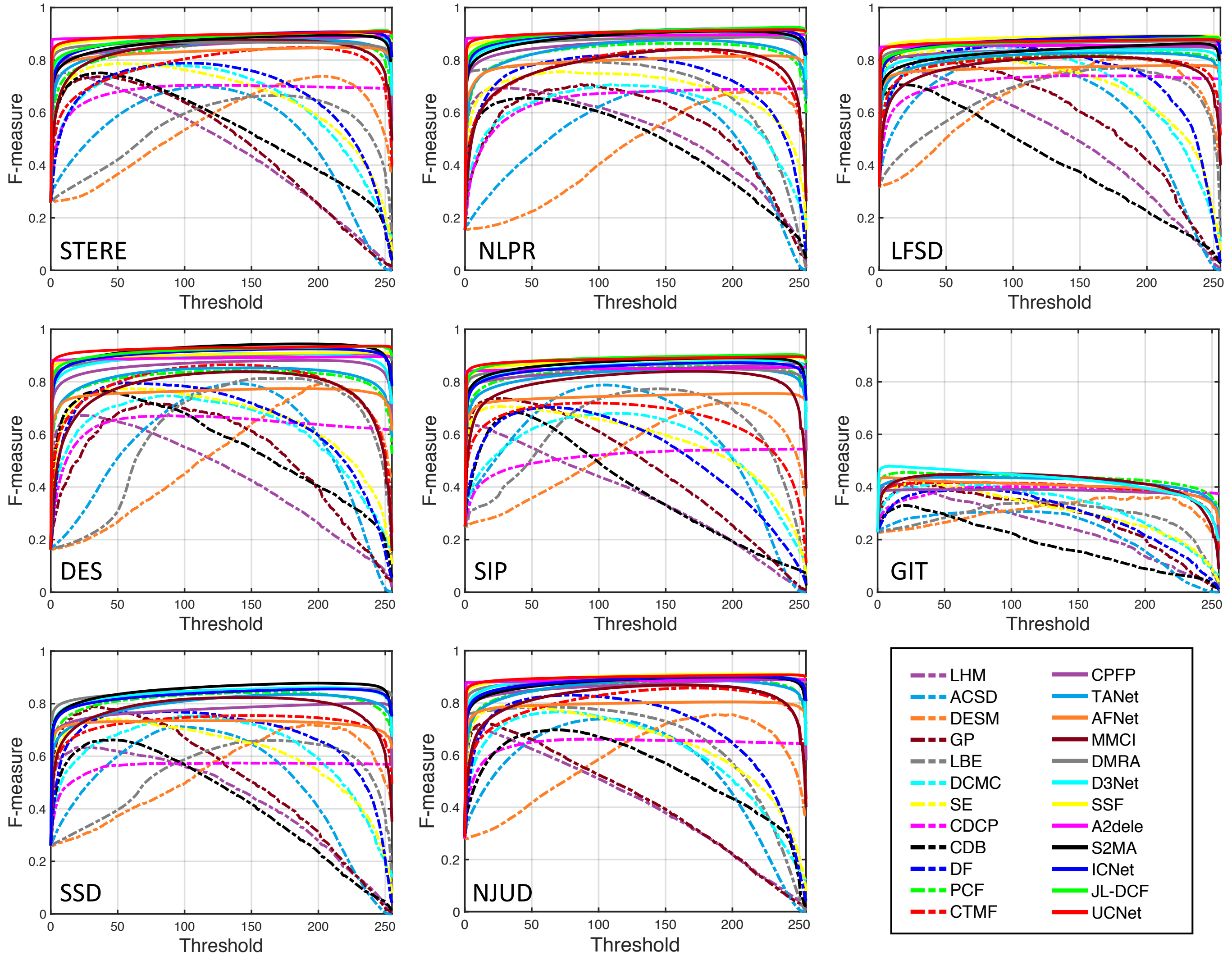

Fig. 7. F-measures under different thresholds for 24 RGB-D based models on the STERE [138], NLPR [51], LFSD [139], DES [49], SIP [3], GIT [47], SSD [85], and NJUD [56] datasets.

TABLE IX
ATTRIBUTE-BASED STUDY *w.r.t.* BACKGROUND CLUTTER. COMPARISON RESULTS FOR 24 REPRESENTATIVE RGB-D BASED SOD MODELS (9 TRADITIONAL MODELS AND 15 DEEP LEARNING-BASED MODELS) ARE PROVIDED IN TERMS OF MAE AND S_α. THE THREE BEST RESULTS ARE SHOWN IN RED, BLUE AND GREEN FONTS.

		Traditional models									Deep learning-based models														
	background	LHM [51]	ACSD [56]	DESM [49]	GP [50]	LBE [57]	DCMC [1]	SE [2]	CDCP [84]	CDB [95]	DF [52]	PCF [92]	CTMF [58]	CPFP [53]	TANet [99]	AFNet [102]	MMCI [55]	DMRA [54]	D^3Net [3]	SSF [4]	A2dele [5]	S^2MA [6]	ICNet [7]	JL-DCF [8]	UC-Net [9]
MAE	Simple	.100	.163	.219	.150	.202	.056	.084	.028	.136	.045	.031	.053	.018	.033	.031	.041	.028	.017	.012	.010	.016	.013	.014	.013
	Uncertain	.164	.195	.294	.175	.210	.140	.133	.139	.159	.129	.062	.081	.050	.059	.075	.070	.058	.045	.043	.043	.049	.041	.037	.037
	Complex	.159	.190	.349	.180	.205	.190	.147	.236	.143	.163	.085	.110	.079	.077	.108	.094	.087	.071	.065	.070	.072	.079	.063	.065
	Overall	.160	.193	.295	.174	.209	.140	.132	.141	.157	.127	.063	.082	.051	.059	.076	.070	.059	.046	.043	.043	.049	.043	.038	.038
S_α	Simple	.781	.787	.761	.694	.748	.930	.856	.941	.704	.944	.944	.913	.958	.937	.922	.933	.935	.960	.966	.965	.965	.969	.961	.962
	Uncertain	.572	.694	.638	.606	.695	.736	.723	.727	.610	.774	.873	.853	.882	.873	.818	.868	.854	.900	.894	.884	.895	.910	.909	.907
	Complex	.496	.627	.509	.545	.616	.577	.605	.487	.575	.627	.782	.742	.787	.790	.694	.768	.751	.822	.815	.786	.813	.808	.829	.833
	Overall	.576	.693	.633	.606	.691	.732	.720	.718	.612	.770	.869	.847	.878	.869	.813	.863	.850	.896	.891	.879	.892	.904	.904	.904

main advantages for the six models below.

• D^3Net [3] consists of two key components, *i.e.*, a three-stream feature learning module and a depth depurator unit. In the three-stream feature learning module, there are three subnetworks, *i.e.*, RgbNet, RgbdNet, and DepthNet. The RgbNet and DepthNet are used to learn high-level feature representations for RGB and depth images, respectively, while the RgbdNet is used to learn their fused representations. It is worth noting that this three-stream feature learning module can capture modality-specific information as well as the correlation between modalities. Thus, balancing the two aspects is very important for multi-modal learning and it has helped to improve the SOD performance. Besides, the depth depurator unit acts as a gate to explicitly filter out low-quality depth maps, which several existing methods do not consider the effects. Because low-quality depth maps can inhibit the fusion between RGB images and depth maps, thus the depth depurator unit can ensure effective multi-modal fusion to achieve robust SOD performance.

• In JL-DCF [8], there are two key components, *i.e.*, a joint learning (JL) and a densely-cooperative fusion (DCF). Specifically, the JL module is used to learn robust saliency features, while the DCF module is used for complementary feature discovery. It is worth noting that this method uses a middle-fusion strategy to extract deep hierarchical features from RGB images and depth maps, in which the cross-modal complementarity can be effectively exploited to achieve accurate prediction.

• In UC-Net [9], instead of producing a single saliency prediction, this model produces multiple predictions by modeling the distribution of the feature output space as a generative model conditioned on RGB-D images. Because each person has some specific preferences in labeling a saliency map, it could fail to capture the stochastic characteristic of saliency while only a single saliency map is produced for an image pair using a deterministic learning pipeline. Thus, the strategy in this model can take into account human uncertainty in saliency annotations. Moreover, considering the fact that depth maps could suffer from noise, directly fusing RGB images and depth maps could cause the network to fit to this noise. Therefore, a depth correction network, designed as an auxiliary component, is proposed to refine depth information with a semantic guided loss. Thus, the above key components are all helpful for improving SOD performance.

• In SSF [4], a complementary interaction module (CIM) is developed to explore discriminative cross-modal complementarities and fuse cross-modal features, where a region-wise attention is introduced to supplement rich boundary information for each modality. Besides, a compensation-aware loss is proposed to improve the network's confidence for hard samples in unreliable depth maps. Thus, these key components enable the proposed model to effectively explore and establish the complementarity of cross-modal feature representations, while at the same time reducing the negative effects introduced by low-quality depth maps, boosting SOD performance.

• In ICNet [7], an information conversion module is proposed to interactively and adaptively explore the correlations between high-level RGB and depth features. Besides, a cross-modal depth-weighted combination block is introduced to enhance the difference between the RGB and depth features in each level, which ensures that the features are treated differently. It is also worth noting that ICNet exploits the complementarity of cross-modal features, as well as explores the continuity of cross-level features, both of which are helpful for achieving accurate predictions.

• In S^{2}MA [6], a self-mutual attention module (SAM) is proposed to fuse RGB and depth images, integrating self-attention and each other's attention to propagate context more accurately. The SAM can provide additional complementary information from multi-modal data to improve SOD performance, overcoming the limitations of the original self-attention, which only uses a single modality. Besides, to reduce the low-quality (*e.g.*, noise) effects of depth cues, a selection mechanism is proposed to reweight the mutual attention. This mechanism can filter out unreliable information, resulting in more accurate saliency prediction.

Fig. 8. Sample images with different objects scales. The scale ratios are denoted in yellow.

2) Attribute-based Evaluation: To investigate the influence of different factors, such as object scale, background clutter, number of salient objects, indoor or outdoor scene, background objects, and lighting conditions, we carry out diverse attribute-based evaluations on several representative RGB-D based SOD models.

• **Object Scale**. To characterize the scale of a salient object area, we compute the ratio between the size of the salient area and the whole image. We define three types of object scales: 1) when the ratio is less than 0.1, it is denoted as "small"; 2) when the ratio is larger than 0.4, it is denoted as "large"; and 3) when the ratio is in the range of $[0.1, 0.4]$, it is denoted as "medium". In this evaluation, we build a hybrid dataset with 2,464 images collected from STERE [138], NLPR [51] , LFSD [139], DES [49], and SIP [3], where 24%, 69.2% and 6.8% of images have small, medium, and large salient object areas, respectively. The constructed hybrid dataset can be found at https://github.com/taozh2017/RGBD-SODsurvey. Some sample images with different object scales are shown in Fig. 8. The comparison results of the attribute-based study *w.r.t.* object scale are shown in Tab. VIII. From the results, it can be observed that all comparison methods obtain better performance in detecting small salient objects while they obtain worse performance in detecting large salient objects. Besides, the three most recent models, *i.e.*, JL-DCF [8], UC-Net [9], and S^{2}MA [6], obtain the best performance. D^{3}Net [3], SSF [4], A2dele [5], and ICNet [7] also obtain promising performance.

• **Background Clutter**. It is difficult to directly characterize background clutter. Since classic SOD methods tend to use prior information or color contrast to locate salient objects, they often fail under complex backgrounds. Thus, in this evaluation, we utilize five traditional SOD methods, *i.e.*, BSCA

TABLE X
ATTRIBUTE-BASED STUDY *w.r.t.* BACKGROUND OBJECTS (*i.e.*, CAR, BARRIER, FLOWER, GRASS, ROAD, SIGN, TREE, AND OTHER). THE COMPARISON METHODS INCLUDING 24 REPRESENTATIVE RGB-D BASED SOD MODELS (9 TRADITIONAL MODELS AND 15 DEEP LEARNING-BASED MODELS) EVALUATED ON THE SIP DATASET [3] IN TERMS OF MAE AND S_α. THE THREE BEST RESULTS ARE SHOWN IN RED, BLUE AND GREEN FONTS.

		Traditional models									Deep learning-based models														
	Categories	LHM [51]	ACSD [56]	DESM [49]	GP [50]	LBE [57]	DCMC [1]	SE [2]	CDCP [84]	CDB [95]	DF [52]	PCF [92]	CTMF [58]	CPFP [53]	TANet [99]	AFNet [102]	MMCI [55]	DMRA [54]	D^{3}Net [3]	SSF [4]	A2dele [5]	S^{2}MA [6]	ICNet [7]	JL-DCF [8]	UC-Net [9]
MAE	Car	.158	.163	.301	.159	.201	.185	.154	.202	.171	.171	.085	.134	.094	.084	.101	.093	.069	.061	.063	.078	.055	.067	.058	.057
	Barrier	.197	.177	.308	.180	.201	.196	.176	.251	.203	.202	.073	.149	.060	.078	.128	.089	.093	.068	.054	.074	.057	.075	.052	.053
	Flower	.105	.122	.306	.099	.186	.158	.063	.141	.101	.132	.091	.075	.133	.100	.090	.081	.046	.095	.107	.051	.104	.025	.054	.075
	Grass	.164	.161	.279	.155	.184	.167	.138	.182	.176	.167	.041	.110	.035	.048	.088	.059	.056	.037	.030	.046	.033	.043	.023	.029
	Road	.189	.167	.281	.176	.187	.181	.164	.225	.189	.169	.070	.140	.054	.072	.125	.078	.093	.059	.049	.072	.050	.065	.045	.044
	Sign	.107	.126	.268	.110	.184	.126	.079	.134	.118	.096	.058	.101	.063	.060	.077	.083	.051	.055	.051	.054	.048	.054	.050	.057
	Tree	.192	.193	.310	.190	.241	.194	.183	.230	.219	.205	.083	.157	.083	.091	.132	.109	.106	.083	.067	.074	.092	.097	.063	.071
	Other	.246	.217	.329	.224	.229	.216	.229	.274	.233	.233	.106	.177	.111	.111	.170	.124	.140	.095	.083	.099	.100	.100	.084	.086
	Overall	.184	.172	.298	.173	.200	.186	.164	.224	.192	.185	.071	.139	.064	.075	.118	.086	.085	.063	.053	.070	.057	.069	.049	.051
S_α	Car	.516	.731	.590	.603	.714	.671	.591	.613	.546	.631	.811	.726	.786	.807	.736	.813	.817	.856	.845	.804	.870	.846	.855	.859
	Barrier	.497	.727	.609	.575	.728	.672	.612	.553	.552	.643	.837	.698	.860	.831	.708	.830	.792	.855	.874	.821	.871	.848	.876	.875
	Flower	.477	.775	.573	.673	.703	.707	.772	.667	.639	.750	.771	.738	.714	.760	.688	.785	.824	.789	.768	.845	.804	.901	.856	.811
	Grass	.537	.756	.643	.605	.760	.728	.683	.672	.559	.672	.908	.770	.908	.899	.780	.888	.876	.917	.924	.878	.928	.910	.939	.924
	Road	.521	.739	.634	.598	.751	.685	.641	.595	.576	.680	.851	.722	.871	.848	.705	.847	.807	.873	.885	.832	.885	.868	.889	.892
	Sign	.578	.786	.634	.628	.719	.745	.761	.714	.615	.757	.855	.756	.833	.857	.771	.818	.848	.849	.849	.842	.871	.861	.859	.840
	Tree	.505	.699	.606	.577	.661	.648	.600	.588	.543	.625	.802	.679	.804	.778	.691	.779	.748	.806	.837	.807	.800	.788	.848	.825
	Other	.460	.687	.594	.532	.706	.669	.563	.554	.542	.600	.786	.677	.774	.782	.647	.790	.722	.800	.828	.785	.809	.799	.821	.823
	Overall	.511	.732	.616	.588	.727	.683	.628	.595	.557	.653	.842	.716	.850	.835	.720	.833	.806	.860	.874	.828	.872	.854	.880	.875

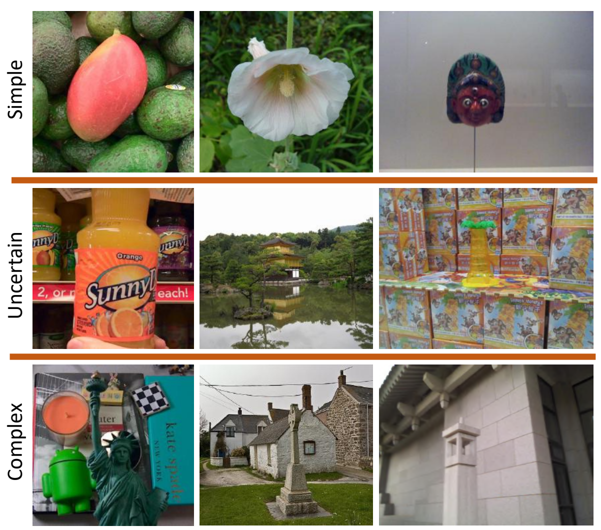

Fig. 9. Sample images with three types of background clutter.

Fig. 10. Sample images with single or multiple salient objects.

[161], CLC [162], MDC [163], MIL [164], and WFD [165], to first detect salient objects in various images and then group these images into different categories (*e.g.*, simple or complex background) according to the results. Specifically, we first construct a hybrid dataset with 1,400 images collected from three datasets (STERE [138], NLPR [51], and LFSD [139]). Then, we apply the five models to this dataset and obtain the S_α values for each, which we use to characterize images as follows: 1) If all S_α values are higher than 0.9, the image is denoted as having a "simple" background; 2) If all S_α values are lower than 0.6, the image is said to have a "complex" background; 3) The remaining images are denoted as "uncertain". Some example images with the three types of background clutter are shown in Fig. 9. The constructed hybrid dataset can be found at https://github.com/taozh2017/RGBD-SODsurvey. The comparison results of the attribute-based study *w.r.t.* background clutter are shown in Tab. IX. As can be seen, all models obtain worse SOD performance on images containing complex backgrounds than simple ones. Among the representative models, JL-DCF [8], UC-Net [9] and SSF [4] achieve the top-three best results. Besides, the four most recent models, *i.e.*, D^{3}Net [3], S^{2}MA [6], A2dele [5], and ICNet [7], also obtain better performance than the other models.

• **Single vs. Multiple Objects**. In this evaluation, we construct a hybrid dataset with 1,229 images collected from the NLPR [51] and SIP [3] datasets. Some example images with single or multiple salient objects are shown in Fig. 10. The comparison results are shown in Fig. 11. From the results,

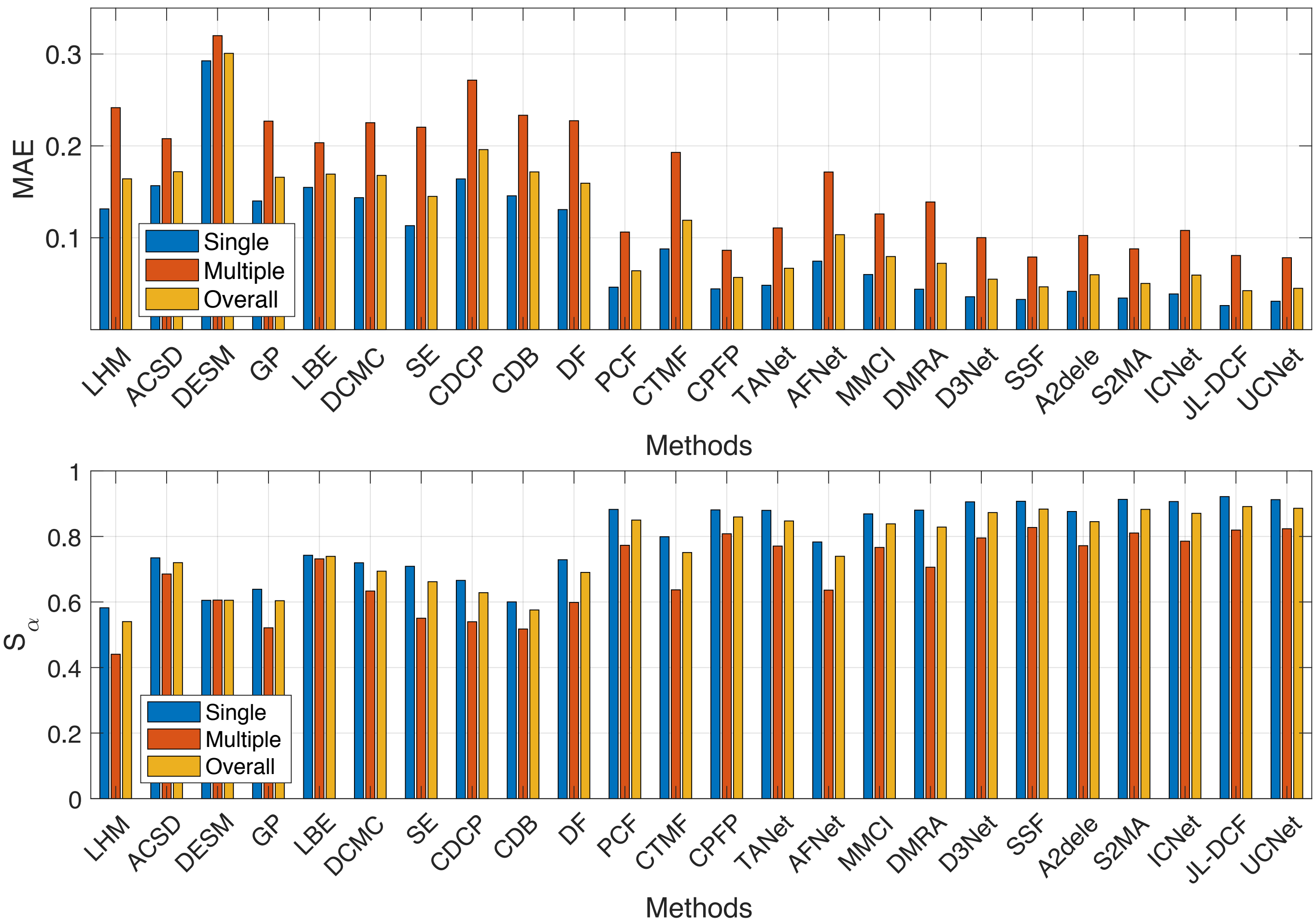

Fig. 11. Attribute-based study *w.r.t.* number of salient objects (*i.e.*, single vs. multiple (multi)). The comparison results on 24 representative RGB-D based SOD models (*i.e.*, LHM [51], ACSD [56], DESM [49], GP [50], LBE [57], DCMC [1], SE [2], CDCP [84], CDB [95], DF [52], PCF [92], CTMF [58], CPFP [53], TANet [99], AFNet [102], MMCI [55], DMRA [54], D^{3}Net [3], SSF [4], A2dele [5], S^{2}MA [6], ICNet [7], JL-DCF [8], and UC-Net [9]) are given in terms of MAE (top) and S_α (bottom).

TABLE XI

ATTRIBUTE-BASED STUDY *w.r.t.* LIGHT CONDITIONS (SUNNY VS. LOW-LIGHT). THE COMPARISON METHODS INCLUDE 24 REPRESENTATIVE RGB-D BASED SOD MODELS (9 TRADITIONAL MODELS AND 15 DEEP LEARNING-BASED MODELS) EVALUATED ON THE SIP DATASET [3] IN TERMS OF MAE AND S_α. THE THREE BEST RESULTS ARE SHOWN IN RED, BLUE AND GREEN FONTS.

		Traditional models									Deep learning-based models														
	Conditions	LHM [51]	ACSD [56]	DESM [49]	GP [50]	LBE [57]	DCMC [1]	SE [2]	CDCP [84]	CDB [95]	DF [52]	PCF [92]	CTMF [58]	CPFP [53]	TANet [99]	AFNet [102]	MMCI [55]	DMRA [54]	D^{3}Net [3]	SSF [4]	A2dele [5]	S^{2}MA [6]	ICNet [7]	JL-DCF [8]	UC-Net [9]
MAE	Sunny	.182	.171	.294	.171	.200	.183	.160	.218	.190	.181	.069	.137	.062	.075	.116	.085	.083	.062	.052	.068	.057	.068	.048	.051
	Low-light	.198	.178	.323	.187	.201	.207	.193	.268	.208	.211	.078	.154	.073	.076	.130	.091	.103	.067	.059	.080	.058	.081	.059	.055
	Overall	.184	.172	.298	.173	.200	.186	.164	.224	.192	.185	.071	.139	.064	.075	.118	.086	.085	.063	.053	.070	.057	.069	.049	.051
S_α	Sunny	.516	.733	.622	.593	.728	.690	.639	.607	.560	.660	.843	.718	.852	.834	.723	.833	.811	.861	.875	.831	.872	.856	.882	.876
	low-light	.481	.721	.573	.554	.722	.635	.556	.515	.543	.610	.838	.701	.838	.837	.700	.832	.775	.855	.867	.810	.871	.839	.867	.871
	Overall	.511	.732	.616	.588	.727	.683	.628	.595	.557	.653	.842	.716	.850	.835	.720	.833	.806	.860	.874	.828	.872	.854	.880	.875

we can see that it is easier to detect single salient object than multiple ones.

• **Indoor vs. Outdoor**. We evaluate the performance of different RGB-D based SOD models on indoor and outdoor scenes. In this evaluation, we construct a hybrid dataset collected from the DES [49], NLPR [51], and LFSD [139] datasets. The comparison results are shown in Fig. 12. From the results, it can be seen that most models struggle more to detect salient objects in indoor scene than outdoor scenes. This is possibly because indoor environments often have varying light conditions.

• **Background Objects**. We evaluate the performance of the RGB-D based SOD models when different background objects are present. We use the SIP dataset [3], and split it into nine categories, *i.e.*, car, barrier, flower, grass, road, sign, tree, and other. The comparison results are shown in Tab. X. As can be seen, all methods obtain diverse performances under different background objects. Among the 24 representative RGB-D based models, JL-DCF [8], UC-Net [9] and SSF [4] achieve the top-three best results. In addition, the four most

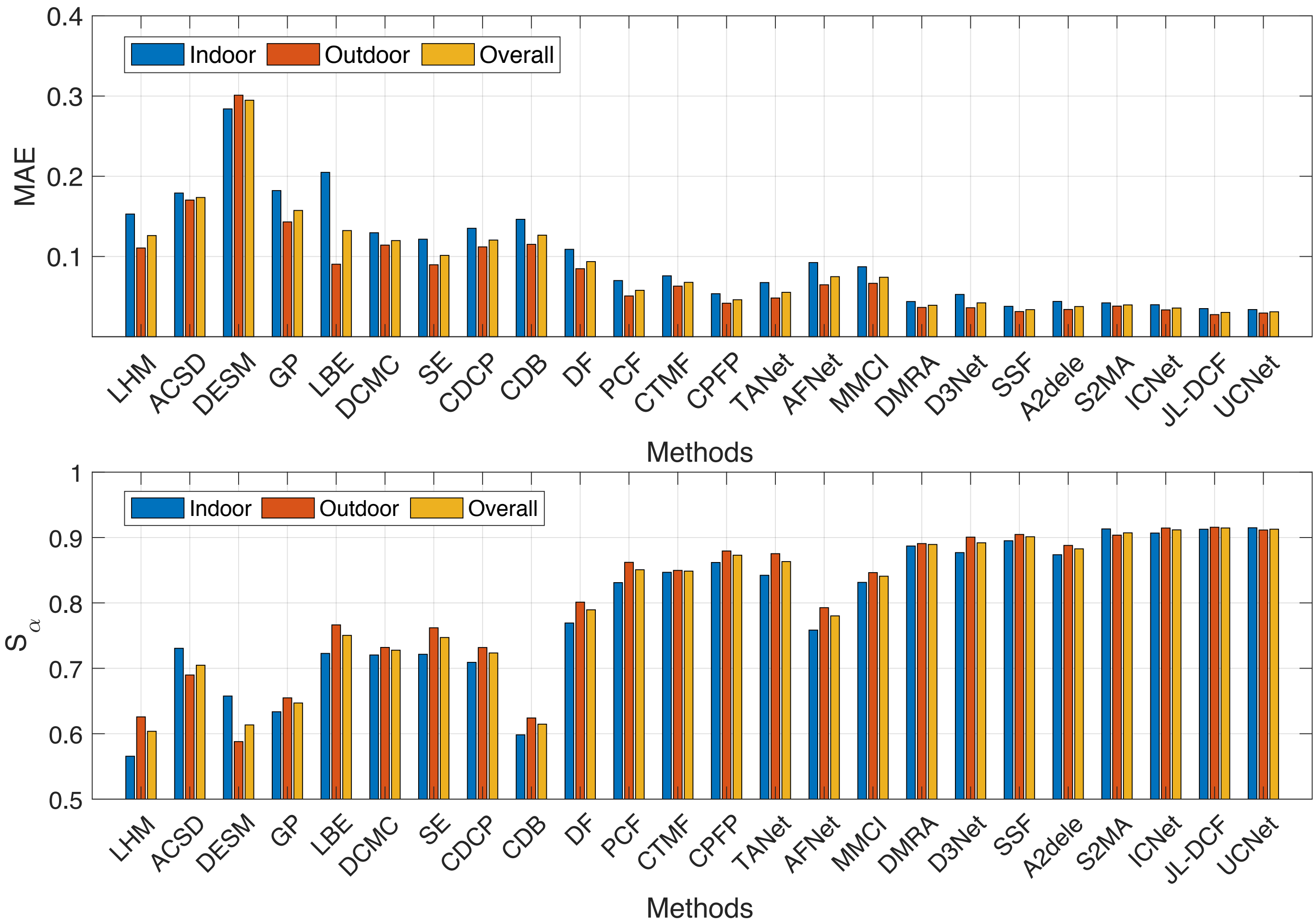

Fig. 12. Attribute-based study *w.r.t.* indoor vs. outdoor environments. The comparison results for 24 representative RGB-D based SOD models (*i.e.*, LHM [51], ACSD [56], DESM [49], GP [50], LBE [57], DCMC [1], SE [2], CDCP [84], CDB [95], DF [52], PCF [92], CTMF [58], CPFP [53], TANet [99], AFNet [102], MMCI [55], DMRA [54], D^{3}Net [3], SSF [4], A2dele [5], S^{2}MA [6], ICNet [7], JL-DCF [8], and UC-Net [9]) are provided in terms of MAE (top) and S_α (bottom).

recent models, *i.e.*, D^{3}Net [3], S^{2}MA [6], A2dele [5], and ICNet [7] obtain better performance than the others.

• **Lighting Conditions**. The performance of SOD can be affected by different lighting conditions. To determine the performance of different RGB-D based SOD models under different lighting conditions, we conduct an evaluation on the SIP dataset [3], which we split it into two categories, *i.e.*, sunny and low-light. The comparison results are shown in Tab. XI. As can be seen, low-light negatively impacts SOD performance. Among comparison models, UC-Net [9] obtains the best performance under sunny conditions while JL-DCF [8] achieves the best result under low-light condition.

In addition, we report the saliency maps generated for various challenging scenes to visualize the performance of different RGB-D based SOD models. Fig. 13 and Fig. 14 show some representative examples using two classic non-deep methods (DCMC [1] and SE [2]) and eight state-of-the-art CNN-based models (DMRA [54], D^{3}Net [3], SSF [4], A2dele [5], S^{2}MA [6], ICNet [7], JL-DCF [8], and UC-Net [9]). The 1^{st} row shows a small object, while the 2^{nd} row is an example of a large one. The 3^{rd} and 4^{th} rows contain complex backgrounds and boundaries, respectively. The 5^{th} and 6^{th} rows contain multiple salient objects. In the 7^{th} row, there are low-light condition. In the 8^{th} row, the depth map is coarse with very inaccurate object boundaries, which could inhibit the SOD performance. From the results in Fig. 13 and Fig. 14, it can be observed that deep models perform better than non-deep models on these challenging scenes, confirming the powerful expression ability of deep features over handcrafted ones. In addition, D^{3}Net [3], S^{2}MA [6], JL-DCF [8], and UC-Net [9] perform better than other deep models.

VI. Challenges and Open Directions

A. *Effects of Imperfect Depth*

Effects of Low-quality Depth Maps. Depth maps with affluent spatial information have been proven beneficial in detecting salient objects from cluttered backgrounds, while the depth quality also directly affects the subsequent SOD performance. The quality of depth maps varies tremendously across different scenarios due to the limitations of depth sensors, posing a challenge when trying to reduce the effects of low-quality depth maps. However, most existing methods directly fuse RGB images and original raw data from depth maps, without considering the effects of low-quality depth maps. There are a few notable exceptions. For example,

Fig. 13. Visual comparisons for two classical non-deep methods (DCMC [1] and SE [2]) and three state-of-the-art CNN-based models (DMRA [54], D^{3}Net [3], SSF [4]).

in [53], a contrast-enhanced network was proposed to learn enhanced depth maps, which have much higher contrasts compared with the original depths. In [4], a compensation-aware loss was designed to pay more attention to hard samples containing unreliable depth information. Moreover, D^{3}Net [3] uses a depth depurator unit (DDU) to classify depth maps into two classes (*i.e.*, reasonable and low-quality). The DDU also acts as a gate that can filter out the low-quality depth maps. However, the above methods often employ a two-step strategy to achieve depth enhancement and multi-modal fusion [4], [53] or an independent gate operation for filtering out poor depths, which could bring a suboptimal problem. There is thus a need to develop an end-to-end framework that can achieve depth enhancement or adaptively weight the depth maps (*e.g.*, assign low weights to poor depth maps) during multi-modal fusion, which would be more helpful for reducing the effects of low-quality depth maps and boosting SOD performance.

Incomplete Depth Maps. In RGB-D datasets, it is inevitable for there to be some low-quality depth maps due to the limitations of the acquisition devices. As previously discussed, several depth enhancement algorithms have been used to improve the quality of depth maps. However, depth maps that suffer from severe noise or blurred edges, are often discarded. In this case, we have complete RGB images but some samples do not have depth maps, which is similar to the incomplete multi-view/modal learning problem [166]–[170]. Thus, we call it “incomplete RGB-D based SOD”. As current models only focus on the SOD task using complete RGB images and depth maps, we believe this could be a new direction for RGB-D SOD.

Depth Estimation. Depth estimation provides an effective solution to recover high-quality depths and overcome the effects of low-quality depth maps. Various depth estimation approaches [171]–[174] have been developed, which could

Fig. 14. Visual comparisons for five state-of-the-art CNN-based models (A2dele [5], S^2MA [6], ICNet [7], JL-DCF [8], and UC-Net [9]).

be introduced into the RGB-D based SOD task to improve performance.

B. Effective Fusion Strategies

Adversarial Learning-based Fusion. It is important to effectively fuse RGB images and depth maps for RGB-D based SOD. Existing models often employ different fusion strategies (*e.g.*, early fusion, middle fusion, or late fusion) to exploit the correlations between RGB images and depth maps. Recently, generative adversarial networks (GANs) [175] have gained widespread attention for the saliency detection task [176], [177]. In common GAN-based SOD models, a generator takes RGB images as inputs and generates the corresponding saliency maps, while a discriminator is adopted to determine whether a given image is synthetic or ground-truth. GAN-based models could easily be extended to RGB-D SOD, which could be helpful for boosting performance due to their superior feature learning ability. Moreover, GANs could also be used to learn common feature representations for RGB images and depth maps [118], which could help with feature or saliency map fusion and further boost the SOD performance.

Attention-induced Fusion. Attention mechanisms have been widely applied to various deep learning-based tasks [178]–[181], allowing networks to selectively pay attention to a subset of regions for extracting discriminative and powerful features. Besides, co-attention mechanisms have been developed to explore the underlying correlations across multiple modalities, and are widely studied in visual question answering [182], [183] and video object segmentation [184]. Thus, for the RGB-D based SOD task, we could also develop attention-based fusion algorithms to exploit correlations between RGB images and depth cues to improve the performance.

C. Different Supervision Strategies

Existing RGB-D models often use a fully supervised strategy to learn saliency prediction models. However, annotating pixel-level saliency maps is a tedious and time-consuming procedure. To alleviate this issue, there has been increased interest in weakly and semi-supervised learning, which have been applied to salient object detection [185]–[189]. Semi-/weak supervision could also be introduced into RGB-D SOD, by leveraging image-level tags [185] and pseudo pixel-wise annotations [188], [190], for improving the detection performance. Besides, several studies [191], [192] have suggested that models pretrained using self-supervision can effectively be used to achieve better performance. Therefore, we could train saliency prediction models on large amounts of annotated RGB images in a self-supervised manner and then transfer the pretrained models to the RGB-D SOD task.

D. Dataset Collection

Dataset size. Although there are nine public RGB-D datasets for SOD, their size is quite limited, *e.g.*, the maximum size is about 2,000 samples for NJUD [56]. When compared with other RGB-D datasets for generic object detection or action recognition [193], [194], the size of RGB-D datasets for SOD is also very small. Thus, it is essential to develop new large-scale RGB-D datasets that can serve as baselines for future research.

Complex Background & Task-driven Datasets. Most existing RGB-D datasets collect images that contain one salient object or multiple objects but with a relatively clean background. However, real-world applications often suffer from much more complicated situations (*e.g.*, occlusion, appearance change, low illumination, etc), which could decrease the SOD performance. Thus, collecting images with complex background is critical to improve the generalization ability of RGB-D SOD models. Moreover, for some tasks, images with specific salient object(s) must be collected. For example, one important technology is road sign recognition in driver assistance systems, which requires images with road signs to be collected. Thus, it is essential to construct task-driven RGB-D datasets like SIP [3].

E. Model Design for Real-world Scenarios

Some smartphones can capture depth maps (*e.g.*, images in the SIP dataset were captured using Huawei Mate 10). Thus it would be feasible to conduct the SOD task in real-world applications, *e.g.*, on smart devices. However, most existing methods include complicated and deep DNNs to increase the model capacity and achieve better performance, preventing them from being directly applied on real-work platforms. To overcome this, model compression [195], [196] techniques could be used to learn compact RGB-D based SOD models with promising detection accuracy. Moreover, JL-DCF [8] utilizes a shared network to locate salient objects using RGB and depth views, which largely reduces the model parameters and makes real-world applications feasible.

F. Extension to RGB-T SOD

In addition to RGB-D SOD, there are several other methods that fuse different modalities for better detection, such as RGB-T SOD, which integrates RGB and thermal infrared data. Thermal infrared cameras can capture the radiation emitted from any object with a temperature above absolute zero, making thermal infrared images insensitive to illumination conditions [197]. Therefore, thermal images can provide supplementary information to improve SOD performance when salient objects suffer from varying light, reflective light, or shadows. Some RGB-T models [197]–[205] and datasets (VT821 [199], VT1000 [203] and VT5000 [205]) have already been proposed over the past few years. Similar to RGB-D SOD, the key aim of RGB-T SOD is to fuse RGB and thermal infrared images and exploit the correlations between the two modalities. Thus, several advanced multi-modal fusion technologies in RGB-D SOD could be extended to the RGB-T SOD task.

VII. Conclusion

In this paper we present, to the best of our knowledge, the first comprehensive review of RGB-D based SOD models. We first review the models from different perspectives, and then summarize popular RGB-D SOD datasets as well as provide details for each. Considering the fact that light fields also provide depth information, we also review popular light field SOD models and the related benchmark datasets. Next, we provide a comprehensive evaluation of 24 representative RGB-D based SOD models as well as an attribute-based evaluation. Specifically, we perform attribute-based performance analysis by constructing new datasets for the 24 representative RGB-D based SOD models. Moreover, we discuss several challenges and highlight open directions for future research. In addition, we briefly discuss the extension work to RGB-T SOD to improve performance when salient objects suffer from varying light, reflective light, or shadows. Although RGB-D based SOD has made notable progress over the past several decades, there is still significant room for improvement. We hope this survey will generate more interest in this field.

References

[1] Runmin Cong, Jianjun Lei, Changqing Zhang, Qingming Huang, Xiaochun Cao, and Chunping Hou, "Saliency detection for stereoscopic images based on depth confidence analysis and multiple cues fusion," *IEEE Signal Processing Letters*, vol. 23, no. 6, pp. 819–823, 2016.

[2] Jingfan Guo, Tongwei Ren, and Jia Bei, "Salient object detection for RGB-D image via saliency evolution," in *Proceedings of the IEEE International Conference on Multimedia and Expo*. IEEE, 2016, pp. 1–6.

[3] Deng-Ping Fan, Zheng Lin, Zhao Zhang, Menglong Zhu, and Ming-Ming Cheng, "Rethinking RGB-D salient object detection: Models, data sets, and large-scale benchmarks," *IEEE Transactions on Neural Networks and Learning Systems*, 2020.

[4] Miao Zhang, Weisong Ren, Yongri Piao, Zhengkun Rong, and Huchuan Lu, "Select, supplement and focus for RGB-D saliency detection," in *Proceedings of the IEEE Conference on Computer Vision and Pattern Recognition*, 2020.

[5] Yongri Piao, Zhengkun Rong, Miao Zhang, Weisong Ren, and Huchuan Lu, "A2dele: Adaptive and attentive depth distiller for efficient RGB-D salient object detection," *Proceedings of the IEEE Conference on Computer Vision and Pattern Recognition*, 2020.

[6] Nian Liu, Ni Zhang, and Junwei Han, “Learning selective self-mutual attention for RGB-D saliency detection,” in *Proceedings of the IEEE Conference on Computer Vision and Pattern Recognition*, 2020.

[7] Gongyang Li, Zhi Liu, and Haibin Ling, “Icnet: Information conversion network for RGB-D based salient object detection,” *IEEE Transactions on Image Processing*, vol. 29, pp. 4873–4884, 2020.

[8] Keren Fu, Deng-Ping Fan, Ge-Peng Ji, and Qijun Zhao, “Jl-dcf: Joint learning and densely-cooperative fusion framework for RGB-D salient object detection,” *Proceedings of the IEEE Conference on Computer Vision and Pattern Recognition*, 2020.

[9] Jing Zhang, Deng-Ping Fan, Yuchao Dai, Saeed Anwar, Fatemeh Sadat Saleh, Tong Zhang, and Nick Barnes, “Uc-net: uncertainty inspired rgb-d saliency detection via conditional variational autoencoders,” in *Proceedings of the IEEE Conference on Computer Vision and Pattern Recognition*, 2020.

[10] Deng-Ping Fan, Ming-Ming Cheng, Jiang-Jiang Liu, Shang-Hua Gao, Qibin Hou, and Ali Borji, “Salient objects in clutter: Bringing salient object detection to the foreground,” in *Proceedings of the European Conference on Computer Vision*. Springer, 2018, pp. 186–202.

[11] Guang-Yu Nie, Ming-Ming Cheng, Yun Liu, Zhengfa Liang, Deng-Ping Fan, Yue Liu, and Yongtian Wang, “Multi-level context ultra-aggregation for stereo matching,” in *Proceedings of the IEEE Conference on Computer Vision and Pattern Recognition*, 2019, pp. 3283–3291.

[12] Jun-Yan Zhu, Jiajun Wu, Yan Xu, Eric Chang, and Zhuowen Tu, “Unsupervised object class discovery via saliency-guided multiple class learning,” *IEEE Transactions on Pattern Analysis and Machine Intelligence*, vol. 37, no. 4, pp. 862–875, 2014.

[13] Deng-Ping Fan, Tengpeng Li, Zheng Lin, Ge-Peng Ji, Dingwen Zhang, Ming-Ming Cheng, Huazhu Fu, and Jianbing Shen, “Re-thinking co-salient object detection,” *arXiv preprint arXiv:2007.03380*, 2020.

[14] Konstantinos Rapantzikos, Yannis Avrithis, and Stefanos Kollias, “Dense saliency-based spatiotemporal feature points for action recognition,” in *Proceedings of the IEEE Conference on Computer Vision and Pattern Recognition*. IEEE, 2009, pp. 1454–1461.

[15] Deng-Ping Fan, Wenguan Wang, Ming-Ming Cheng, and Jianbing Shen, “Shifting more attention to video salient object detection,” in *Proceedings of the IEEE Conference on Computer Vision and Pattern Recognition*, 2019, pp. 8554–8564.

[16] Wenguan Wang, Jianbing Shen, Ruigang Yang, and Fatih Porikli, “Saliency-aware video object segmentation,” *IEEE Transactions on Pattern Analysis and Machine Intelligence*, vol. 40, no. 1, pp. 20–33, 2017.

[17] Hongmei Song, Wenguan Wang, Sanyuan Zhao, Jianbing Shen, and Kin-Man Lam, “Pyramid dilated deeper convlstm for video salient object detection,” in *Proceedings of the European Conference on Computer Vision*. Springer, 2018, pp. 715–731.

[18] Wenguan Wang, Jianbing Shen, and Ling Shao, “Video salient object detection via fully convolutional networks,” *IEEE Transactions on Image Processing*, vol. 27, no. 1, pp. 38–49, 2017.

[19] Wataru Shimoda and Keiji Yanai, “Distinct class-specific saliency maps for weakly supervised semantic segmentation,” in *Proceedings of the European Conference on Computer Vision*. Springer, 2016, pp. 218–234.

[20] Yu Zeng, Yunzhi Zhuge, Huchuan Lu, and Lihe Zhang, “Joint learning of saliency detection and weakly supervised semantic segmentation,” in *Proceedings of the IEEE International Conference on Computer Vision*. Springer, 2019, pp. 7223–7233.

[21] Deng-Ping Fan, Ge-Peng Ji, Tao Zhou, Geng Chen, Huazhu Fu, Jianbing Shen, and Ling Shao, “Pranet: Parallel reverse attention network for polyp segmentation,” in *Medical Image Computing and Computer-Assisted Intervention*, 2020.

[22] Deng-Ping Fan, Tao Zhou, Ge-Peng Ji, Yi Zhou, Geng Chen, Huazhu Fu, Jianbing Shen, and Ling Shao, “Inf-net: Automatic covid-19 lung infection segmentation from ct images,” *IEEE Transactions on Medical Imaging*, 2020.

[23] Yu-Huan Wu, Shang-Hua Gao, Jie Mei, Jun Xu, Deng-Ping Fan, Chao-Wei Zhao, and Ming-Ming Cheng, “Jcs: An explainable covid-19 diagnosis system by joint classification and segmentation,” *arXiv preprint arXiv:2004.07054*, 2020.

[24] Vijay Mahadevan and Nuno Vasconcelos, “Saliency-based discriminant tracking,” in *Proceedings of the IEEE Conference on Computer Vision and Pattern Recognition*. IEEE, 2009, pp. 1007–1013.

[25] Seunghoon Hong, Tackgeun You, Suha Kwak, and Bohyung Han, “Online tracking by learning discriminative saliency map with convolutional neural network,” in *Proceedings of the International Conference on Machine Learning*, 2015, pp. 597–606.

[26] Rui Zhao, Wanli Oyang, and Xiaogang Wang, “Person re-identification by saliency learning,” *IEEE Transactions on Pattern Analysis and Machine Intelligence*, vol. 39, no. 2, pp. 356–370, 2016.

[27] Niki Martinel, Christian Micheloni, and Gian Luca Foresti, “Kernelized saliency-based person re-identification through multiple metric learning,” *IEEE Transactions on Image Processing*, vol. 24, no. 12, pp. 5645–5658, 2015.

[28] Deng-Ping Fan, Ge-Peng Ji, Guolei Sun, Ming-Ming Cheng, Jianbing Shen, and Ling Shao, “Camouflaged object detection,” in *Proceedings of the IEEE Conference on Computer Vision and Pattern Recognition*, 2020, pp. 2777–2787.

[29] Guanghai Liu and Dengping Fan, “A model of visual attention for natural image retrieval,” in *Proceedings of the IEEE Conference on Information Science and Cloud Computing Companion*. IEEE, 2013, pp. 728–733.

[30] Jia-Xing Zhao, Jiang-Jiang Liu, Deng-Ping Fan, Yang Cao, Jufeng Yang, and Ming-Ming Cheng, “Egnet: Edge guidance network for salient object detection,” in *Proceedings of the IEEE International Conference on Computer Vision*, 2019, pp. 8779–8788.

[31] Wei-Chih Tu, Shengfeng He, Qingxiong Yang, and Shao-Yi Chien, “Real-time salient object detection with a minimum spanning tree,” in *Proceedings of the IEEE conference on Computer Vision and Pattern Recognition*, 2016, pp. 2334–2342.

[32] Changqun Xia, Jia Li, Xiaowu Chen, Anlin Zheng, and Yu Zhang, “What is and what is not a salient object? learning salient object detector by ensembling linear exemplar regressors,” in *Proceedings of the IEEE Conference on Computer Vision and Pattern Recognition*, 2017, pp. 4142–4150.

[33] Xiaodi Hou and Liqing Zhang, “Saliency detection: A spectral residual approach,” in *Proceedings of the IEEE Conference on Computer Vision and Pattern Recognition*. IEEE, 2007, pp. 1–8.

[34] Qiong Yan, Li Xu, Jianping Shi, and Jiaya Jia, “Hierarchical saliency detection,” in *Proceedings of the IEEE Conference on Computer Vision and Pattern Recognition*, 2013, pp. 1155–1162.

[35] Chuan Yang, Lihe Zhang, Huchuan Lu, Xiang Ruan, and Ming-Hsuan Yang, “Saliency detection via graph-based manifold ranking,” in *Proceedings of the IEEE Conference on Computer Vision and Pattern Recognition*, 2013, pp. 3166–3173.

[36] Guanbin Li and Yizhou Yu, “Deep contrast learning for salient object detection,” in *Proceedings of the IEEE Conference on Computer Vision and Pattern Recognition*, 2016, pp. 478–487.

[37] Dingwen Zhang, Deyu Meng, and Junwei Han, “Co-saliency detection via a self-paced multiple-instance learning framework,” *IEEE Transactions on Pattern Analysis and Machine Intelligence*, vol. 39, no. 5, pp. 865–878, 2016.

[38] Pingping Zhang, Dong Wang, Huchuan Lu, Hongyu Wang, and Xiang Ruan, “Amulet: Aggregating multi-level convolutional features for salient object detection,” in *Proceedings of the IEEE International Conference on Computer Vision*, 2017, pp. 202–211.

[39] Pingping Zhang, Dong Wang, Huchuan Lu, Hongyu Wang, and Baocai Yin, “Learning uncertain convolutional features for accurate saliency detection,” in *Proceedings of the IEEE International Conference on Computer Vision*, 2017, pp. 212–221.

[40] Tiantian Wang, Ali Borji, Lihe Zhang, Pingping Zhang, and Huchuan Lu, “A stagewise refinement model for detecting salient objects in images,” in *Proceedings of the IEEE International Conference on Computer Vision*, 2017, pp. 4019–4028.

[41] Xin Li, Fan Yang, Hong Cheng, Wei Liu, and Dinggang Shen, “Contour knowledge transfer for salient object detection,” in *Proceedings of the Proceedings of the European Conference on Computer Vision*. Springer, September 2018.

[42] Wenguan Wang, Shuyang Zhao, Jianbing Shen, Steven CH Hoi, and Ali Borji, “Salient object detection with pyramid attention and salient edges,” in *Proceedings of the IEEE Conference on Computer Vision and Pattern Recognition*, 2019, pp. 1448–1457.

[43] Jinming Su, Jia Li, Yu Zhang, Changqun Xia, and Yonghong Tian, “Selectivity or invariance: Boundary-aware salient object detection,” in *Proceedings of the IEEE International Conference on Computer Vision*, 2019, pp. 3799–3808.

[44] Ting Zhao and Xiangqian Wu, “Pyramid feature attention network for saliency detection,” in *Proceedings of the IEEE Conference on Computer Vision and Pattern Recognition*, 2019, pp. 3085–3094.

[45] Hao Chen and Youfu Li, “Cnn-based rgb-d salient object detection: Learn, select and fuse,” *arXiv preprint arXiv:1909.09309*, 2019.

[46] Congyan Lang, Tam V Nguyen, Harish Katti, Karthik Yadati, Mohan Kankanhalli, and Shuicheng Yan, “Depth matters: Influence of depth

cues on visual saliency," in *Proceedings of the European Conference on Computer Vision*. Springer, 2012, pp. 101–115.

[47] Arridhana Ciptadi, Tucker Hermans, and James M Rehg, "An in depth view of saliency," Georgia Institute of Technology, 2013.

[48] Karthik Desingh, K Madhava Krishna, Deepu Rajan, and CV Jawahar, "Depth really matters: Improving visual salient region detection with depth," in *Proceedings of the British Machine Vision Conference*, 2013.

[49] Yupeng Cheng, Huazhu Fu, Xingxing Wei, Jiangjian Xiao, and Xiaochun Cao, "Depth enhanced saliency detection method," in *Proceedings of the International Conference on Internet Multimedia Computing and Service*, 2014, pp. 23–27.

[50] Jianqiang Ren, Xiaojin Gong, Lu Yu, Wenhui Zhou, and Michael Ying Yang, "Exploiting global priors for RGB-D saliency detection," in *Proceedings of the IEEE Conference on Computer Vision and Pattern Recognition Workshops*, 2015, pp. 25–32.

[51] Houwen Peng, Bing Li, Weihua Xiong, Weiming Hu, and Rongrong Ji, "Rgbd salient object detection: a benchmark and algorithms," in *Proceedings of the European Conference on Computer Vision*. Springer, 2014, pp. 92–109.

[52] Liangqiong Qu, Shengfeng He, Jiawei Zhang, Jiandong Tian, Yandong Tang, and Qingxiong Yang, "RGBD salient object detection via deep fusion," *IEEE Transactions on Image Processing*, vol. 26, no. 5, pp. 2274–2285, 2017.

[53] Jia-Xing Zhao, Yang Cao, Deng-Ping Fan, Ming-Ming Cheng, Xuan-Yi Li, and Le Zhang, "Contrast prior and fluid pyramid integration for RGBD salient object detection," in *Proceedings of the IEEE Conference on Computer Vision and Pattern Recognition*, 2019, pp. 3927–3936.

[54] Yongri Piao, Wei Ji, Jingjing Li, Miao Zhang, and Huchuan Lu, "Depth-induced multi-scale recurrent attention network for saliency detection," in *Proceedings of the IEEE International Conference on Computer Vision*, 2019, pp. 7254–7263.

[55] Hao Chen, Youfu Li, and Dan Su, "Multi-modal fusion network with multi-scale multi-path and cross-modal interactions for RGB-D salient object detection," *Pattern Recognition*, vol. 86, pp. 376–385, 2019.

[56] Ran Ju, Ling Ge, Wenjing Geng, Tongwei Ren, and Gangshan Wu, "Depth saliency based on anisotropic center-surround difference," in *Proceedings of the IEEE International Conference on Image Processing*. IEEE, 2014, pp. 1115–1119.

[57] David Feng, Nick Barnes, Shaodi You, and Chris McCarthy, "Local background enclosure for RGB-D salient object detection," in *Proceedings of the IEEE Conference on Computer Vision and Pattern Recognition*, 2016, pp. 2343–2350.

[58] Junwei Han, Hao Chen, Nian Liu, Chenggang Yan, and Xuelong Li, "Cnns-based RGB-D saliency detection via cross-view transfer and multiview fusion," *IEEE Transactions on Cybernetics*, vol. 48, no. 11, pp. 3171–3183, 2017.

[59] Ali Borji, Ming-Ming Cheng, Huaizu Jiang, and Jia Li, "Salient object detection: A benchmark," *IEEE Transactions on Image Processing*, vol. 24, no. 12, pp. 5706–5722, 2015.

[60] Runmin Cong, Jianjun Lei, Huazhu Fu, Ming-Ming Cheng, Weisi Lin, and Qingming Huang, "Review of visual saliency detection with comprehensive information," *IEEE Transactions on Circuits and Systems for Video Technology*, vol. 29, no. 10, pp. 2941–2959, 2018.

[61] Dingwen Zhang, Huazhu Fu, Junwei Han, Ali Borji, and Xuelong Li, "A review of co-saliency detection algorithms: Fundamentals, applications, and challenges," *ACM Transactions on Intelligent Systems and Technology*, vol. 9, no. 4, pp. 1–31, 2018.

[62] Junwei Han, Dingwen Zhang, Gong Cheng, Nian Liu, and Dong Xu, "Advanced deep-learning techniques for salient and category-specific object detection: a survey," *IEEE Signal Processing Magazine*, vol. 35, no. 1, pp. 84–100, 2018.

[63] Tam V Nguyen, Qi Zhao, and Shuicheng Yan, "Attentive systems: A survey," *International Journal of Computer Vision*, vol. 126, no. 1, pp. 86–110, 2018.

[64] Ali Borji, Ming-Ming Cheng, Qibin Hou, Huaizu Jiang, and Jia Li, "Salient object detection: A survey," *Computational Visual Media*, pp. 1–34, 2014.

[65] Zhong-Qiu Zhao, Peng Zheng, Shou-tao Xu, and Xindong Wu, "Object detection with deep learning: A review," *IEEE Transactions on Neural Networks and Learning Systems*, vol. 30, no. 11, pp. 3212–3232, 2019.

[66] Wenguan Wang, Qiuxia Lai, Huazhu Fu, Jianbing Shen, Haibin Ling, and Ruigang Yang, "Salient object detection in the deep learning era: An in-depth survey," *arXiv preprint arXiv:1904.09146*, 2019.

[67] Hailong Zhang, Jianjun Lei, Xiaohong Fan, Meimin Wu, Peng Zhang, and Shupo Bu, "Depth combined saliency detection based on region contrast model," in *Proceedings of International Conference on Computer Science & Education*. IEEE, 2012, pp. 763–766.

[68] Jianjun Lei, Hailong Zhang, Lei You, Chunping Hou, and Laihua Wang, "Evaluation and modeling of depth feature incorporated visual attention for salient object segmentation," *Neurocomputing*, vol. 120, pp. 24–33, 2013.

[69] Xingxing Fan, Zhi Liu, and Guangling Sun, "Salient region detection for stereoscopic images," in *Proceedings of the International Conference on Digital Signal Processing*. IEEE, 2014, pp. 454–458.

[70] Jingfan Guo, Tongwei Ren, Jia Bei, and Yujin Zhu, "Salient object detection in rgb-d image based on saliency fusion and propagation," in *Proceedings of the International Conference on Internet Multimedia Computing and Service*, 2015, pp. 1–5.

[71] Yanlong Tang, Ruofeng Tong, Min Tang, and Yun Zhang, "Depth incorporating with color improves salient object detection," *The Visual Computer*, vol. 32, no. 1, pp. 111–121, 2016.

[72] Lixing Jiang, Artur Koch, and Andreas Zell, "Salient regions detection for indoor robots using rgb-d data," in *Proceedings of the IEEE International Conference on Robotics and Automation*. IEEE, 2015, pp. 1323–1328.

[73] Haoyang Xue, Yun Gu, Yijun Li, and Jie Yang, "Rgb-d saliency detection via mutual guided manifold ranking," in *Proceedings of IEEE International Conference on Image Processing*. IEEE, 2015, pp. 666–670.

[74] Lei Zhu, Zhiguo Cao, Zhiwen Fang, Yang Xiao, Jin Wu, Huiping Deng, and Jing Liu, "Selective features for rgb-d saliency," in *Proceedings of Chinese Automation Congress*. IEEE, 2015, pp. 512–517.

[75] Huan Du, Zhi Liu, Hangke Song, Lin Mei, and Zheng Xu, "Improving RGBD saliency detection using progressive region classification and saliency fusion," *IEEE Access*, vol. 4, pp. 8987–8994, 2016.

[76] Song-Tao Wang, Zhen Zhou, Han-Bing Qu, and Bin Li, "Rgb-d saliency detection under bayesian framework," in *Proceedings of International Conference on Pattern Recognition*. IEEE, 2016, pp. 1881–1886.

[77] Hao Sheng, Xiaoyu Liu, and Shuo Zhang, "Saliency analysis based on depth contrast increased," in *Proceedings of IEEE International Conference on Acoustics, Speech and Signal Processing*. IEEE, 2016, pp. 1347–1351.

[78] Hangke Song, Zhi Liu, Huan Du, and Guangling Sun, "Depth-aware saliency detection using discriminative saliency fusion," in *Proceedings of IEEE International Conference on Acoustics, Speech and Signal Processing*. IEEE, 2016, pp. 1626–1630.

[79] Song-Tao Wang, Zhen Zhou, Han-Bing Qu, and Bin Li, "Visual saliency detection for RGB-D images with generative model," in *Proceedings of the Asian Conference on Computer Vision*. Springer, 2016, pp. 20–35.

[80] David Feng, Nick Barnes, and Shaodi You, "Hoso: Histogram of surface orientation for rgb-d salient object detection," in *Proceedings of the International Conference on Digital Image Computing: Techniques and Applications*. IEEE, 2017, pp. 1–8.

[81] Hao Chen, You-Fu Li, and Dan Su, "M3net: Multi-scale multi-path multi-modal fusion network and example application to rgb-d salient object detection," in *Proceedings of IEEE/RSJ International Conference on Intelligent Robots and Systems*. IEEE, 2017, pp. 4911–4916.

[82] Hao Chen, Youfu Li, and Dan Su, "RGB-D saliency detection by multi-stream late fusion network," in *Proceedings of the International Conference on Computer Vision Systems*. Springer, 2017, pp. 459–468.

[83] Riku Shigematsu, David Feng, Shaodi You, and Nick Barnes, "Learning RGB-D salient object detection using background enclosure, depth contrast, and top-down features," in *Proceedings of the IEEE International Conference on Computer Vision Workshops*, 2017, pp. 2749–2757.

[84] Chunbiao Zhu, Ge Li, Wenmin Wang, and Ronggang Wang, "An innovative salient object detection using center-dark channel prior," in *Proceedings of the IEEE International Conference on Computer Vision Workshops*, 2017, pp. 1509–1515.

[85] Chunbiao Zhu and Ge Li, "A three-pathway psychobiological framework of salient object detection using stereoscopic technology," in *Proceedings of the IEEE International Conference on Computer Vision Workshops*, 2017, pp. 3008–3014.

[86] Anzhi Wang and Minghui Wang, "RGB-D salient object detection via minimum barrier distance transform and saliency fusion," *IEEE Signal Processing Letters*, vol. 24, no. 5, pp. 663–667, 2017.

[87] Hangke Song, Zhi Liu, Huan Du, Guangling Sun, Olivier Le Meur, and Tongwei Ren, "Depth-aware salient object detection and segmentation via multiscale discriminative saliency fusion and bootstrap learning," *IEEE Transactions on Image Processing*, vol. 26, no. 9, pp. 4204–4216, 2017.

[88] Runmin Cong, Jianjun Lei, Huazhu Fu, Weisi Lin, Qingming Huang, Xiaochun Cao, and Chunping Hou, "An iterative co-saliency framework for RGBD images," *IEEE Transactions on Cybernetics*, vol. 49, no. 1, pp. 233–246, 2017.

[89] Nevrez Imamoglu, Wataru Shimoda, Chi Zhang, Yuming Fang, Asako Kanezaki, Keiji Yanai, and Yoshifumi Nishida, "An integration of bottom-up and top-down salient cues on rgb-d data: saliency from objectness versus non-objectness," *Signal, Image and Video Processing*, vol. 12, no. 2, pp. 307–314, 2018.

[90] Runmin Cong, Jianjun Lei, Huazhu Fu, Qingming Huang, Xiaochun Cao, and Nam Ling, "HSCS: Hierarchical sparsity based co-saliency detection for RGBD images," *IEEE Transactions on Multimedia*, vol. 21, no. 7, pp. 1660–1671, 2018.

[91] Runmin Cong, Jianjun Lei, Huazhu Fu, Qingming Huang, Xiaochun Cao, and Chunping Hou, "Co-saliency detection for RGBD images based on multi-constraint feature matching and cross label propagation," *IEEE Transactions on Image Processing*, vol. 27, no. 2, pp. 568–579, 2017.

[92] Hao Chen and Youfu Li, "Progressively complementarity-aware fusion network for RGB-D salient object detection," in *Proceedings of the IEEE Conference on Computer Vision and Pattern Recognition*, 2018, pp. 3051–3060.

[93] Posheng Huang, Chin-Han Shen, and Hsu-Feng Hsiao, "Rgbd salient object detection using spatially coherent deep learning framework," in *Proceedings of the IEEE International Conference on Digital Signal Processing*. IEEE, 2018, pp. 1–5.

[94] Hao Chen, You-Fu Li, and Dan Su, "Attention-aware cross-modal cross-level fusion network for RGB-D salient object detection," in *Proceedings of the IEEE/RSJ International Conference on Intelligent Robots and Systems*. IEEE, 2018, pp. 6821–6826.

[95] Fangfang Liang, Lijuan Duan, Wei Ma, Yuanhua Qiao, Zhi Cai, and Laiyun Qing, "Stereoscopic saliency model using contrast and depth-guided-background prior," *Neurocomputing*, vol. 275, pp. 2227–2238, 2018.

[96] Zhengyi Liu, Song Shi, Quntao Duan, Wei Zhang, and Peng Zhao, "Salient object detection for RGB-D image by single stream recurrent convolution neural network," *Neurocomputing*, vol. 363, pp. 46–57, 2019.

[97] Chunbiao Zhu, Xing Cai, Kan Huang, Thomas H Li, and Ge Li, "PDNet: Prior-model guided depth-enhanced network for salient object detection," in *Proceedings of the IEEE International Conference on Multimedia and Expo*. IEEE, 2019, pp. 199–204.

[98] Yongri Piao, Xiao Li, Miao Zhang, Jingyi Yu, and Huchuan Lu, "Saliency detection via depth-induced cellular automata on light field," *IEEE Transactions on Image Processing*, vol. 29, pp. 1879–1889, 2020.

[99] Hao Chen and Youfu Li, "Three-stream attention-aware network for RGB-D salient object detection," *IEEE Transactions on Image Processing*, vol. 28, no. 6, pp. 2825–2835, 2019.

[100] Hao Chen, Youfu Li, and Dan Su, "Discriminative cross-modal transfer learning and densely cross-level feedback fusion for RGB-D salient object detection," *IEEE Transactions on Cybernetics*, 2019.

[101] Runmin Cong, Jianjun Lei, Huazhu Fu, Junhui Hou, Qingming Huang, and Sam Kwong, "Going from RGB to RGBD saliency: A depth-guided transformation model," *IEEE Transactions on Cybernetics*, 2019.

[102] Ningning Wang and Xiaojin Gong, "Adaptive fusion for RGB-D salient object detection," *IEEE Access*, vol. 7, pp. 55277–55284, 2019.

[103] Xiaofei Zhou, Gongyang Li, Chen Gong, Zhi Liu, and Jiyong Zhang, "Attention-guided RGBD saliency detection using appearance information," *Image and Vision Computing*, vol. 95, pp. 103888, 2020.

[104] Zhengyi Liu, Wei Zhang, and Peng Zhao, "A cross-modal adaptive gated fusion generative adversarial network for RGB-D salient object detection," *Neurocomputing*, 2020.

[105] Fangfang Liang, Lijuan Duan, Wei Ma, Yuanhua Qiao, Zhi Cai, Jun Miao, and Qixiang Ye, "Cocnn: RGB-D deep fusion for stereoscopic salient object detection," *Pattern Recognition*, p. 107329, 2020.

[106] Chongyi Li, Runmin Cong, Sam Kwong, Junhui Hou, Huazhu Fu, Guopu Zhu, Dingwen Zhang, and Qingming Huang, "ASIF-Net: Attention steered interweave fusion network for RGB-D salient object detection," *IEEE Transactions on Cybernetics*, 2020.

[107] Rui Huang, Yan Xing, and Yaobin Zou, "Triple-complementary network for RGB-D salient object detection," *IEEE Signal Processing Letters*, 2020.

[108] Chenglizhao Chen, Jipeng Wei, Chong Peng, Weizhong Zhang, and Hong Qin, "Improved saliency detection in RGB-D images using two-phase depth estimation and selective deep fusion," *IEEE Transactions on Image Processing*, vol. 29, pp. 4296–4307, 2020.

[109] Rui Huang, Yan Xing, and ZeZheng Wang, "RGB-D salient object detection by a CNN with multiple layers fusion," *IEEE Signal Processing Letters*, vol. 26, no. 4, pp. 552–556, 2019.

[110] Di Liu, Yaosi Hu, Kao Zhang, and Zhenzhong Chen, "Two-stream refinement network for rgb-d saliency detection," in *Proceedings of IEEE International Conference on Image Processing*. IEEE, 2019, pp. 3925–3929.

[111] Huan Du, Zhi Liu, and Ran Shi, "Salient object segmentation based on depth-aware image layering," *Multimedia Tools and Applications*, vol. 78, no. 9, pp. 12125–12138, 2019.

[112] Wujie Zhou, Ying Lv, Jingsheng Lei, and Lu Yu, "Global and local-contrast guides content-aware fusion for rgb-d saliency prediction," *IEEE Transactions on Systems, Man, and Cybernetics: Systems*, 2019.

[113] Chih-Yao Ma and Hsueh-Ming Hang, "Learning-based saliency model with depth information," *Journal of vision*, vol. 15, no. 6, pp. 19–19, 2015.

[114] Zhigang Jin, Jingkun Li, and Dong Li, "Co-saliency detection for rgbd images based on effective propagation mechanism," *IEEE Access*, vol. 7, pp. 141311–141318, 2019.

[115] Yu Ding, Zhi Liu, Mengke Huang, Ran Shi, and Xiangyang Wang, "Depth-aware saliency detection using convolutional neural networks," *Journal of Visual Communication and Image Representation*, vol. 61, pp. 1–9, 2019.

[116] Zuyao Chen and Qingming Huang, "Depth potentiality-aware gated attention network for RGB-D salient object detection," *arXiv preprint arXiv:2003.08608*, 2020.

[117] Yue Wang, Yuke Li, James H Elder, Huchuan Lu, and Runmin Wu, "Synergistic saliency and depth prediction for RGB-D saliency detection," *arXiv preprint arXiv:2007.01711*, 2020.

[118] Bo Jiang, Zitai Zhou, Xiao Wang, Jin Tang, and Bin Luo, "cmsalgan: RGB-D salient object detection with cross-view generative adversarial networks," *IEEE Transactions on Multimedia*, 2020.

[119] Fen Xiao, Bin Li, Yimu Peng, Chunhong Cao, Kai Hu, and Xieping Gao, "Multi-modal weights sharing and hierarchical feature fusion for rgbd salient object detection," *IEEE Access*, vol. 8, pp. 26602–26611, 2020.

[120] Zhao Zhang, Zheng Lin, Jun Xu, Wenda Jin, Shao-Ping Lu, and Deng-Ping Fan, "Bilateral attention network for rgb-d salient object detection," *arXiv preprint arXiv:2004.14582*, 2020.

[121] Wujie Zhou, Yuzhen Chen, Chang Liu, and Lu Yu, "GFNet: Gate fusion network with res2net for detecting salient objects in rgb-d images," *IEEE Signal Processing Letters*, 2020.

[122] Zhengyi Liu, Jiting Tang, Qian Xiang, and Peng Zhao, "Salient object detection for rgb-d images by generative adversarial network," *Multimedia Tools and Applications*, pp. 1–23, 2020.

[123] Gongyang Li, Zhi Liu, Linwei Ye, Yang Wang, and Haibin Ling, "Cross-modal weighting network for rgb-d salient object detection," in *Proceedings of the European Conference on Computer Vision*. Springer, 2020.

[124] Youwei Pang, Lihe Zhang, Xiaoqi Zhao, and Huchuan Lu, "Hierarchical dynamic filtering network for RGB-D salient object detection," in *Proceedings of the European Conference on Computer Vision*. Springer, 2020.

[125] Ao Luo, Xin Li, Fan Yang, Zhicheng Jiao, Hong Cheng, and Siwei Lyu, "Cascade graph neural networks for rgb-d salient object detection," in *Proceedings of the Proceedings of the European Conference on Computer Vision*. Springer, 2020.

[126] Chongyi Li, Runmin Cong, Yongri Piao, Qianqian Xu, and Chen Change Loy, "Rgb-d salient object detection with cross-modality modulation and selection," in *Proceedings of the European Conference on Computer Vision*. Springer, 2020.

[127] Xiaoqi Zhao, Lihe Zhang, Youwei Pang, Huchuan Lu, and Lei Zhang, "A single stream network for robust and real-time rgb-d salient object detection," in *Proceedings of the European Conference on Computer Vision*. Springer, 2020.

[128] Wei Ji, Jingjing Li, Miao Zhang, Yongri Piao, and Huchuan Lu, "Accurate rgb-d salient object detection via collaborative learning," in *ECCV*, 2020.

[129] Deng-Ping Fan, Yingjie Zhai, Ali Borji, Jufeng Yang, and Ling Shao, "Bbs-net: Rgb-d salient object detection with a bifurcated backbone strategy network," in *Proceedings of the European Conference on Computer Vision*. Springer, 2020.

[130] Miao Zhang, Sun Xiao Fei, Jie Liu, Shuang Xu, Yongri Piao, and Huchuan Lu, "Asymmetric two-stream architecture for accurate rgb-d saliency detection," in *Proceedings of the European Conference on Computer Vision*. Springer, 2020.

[131] Shuhan Chen and Yun Fu, "Progressively guided alternate refinement network for rgb-d salient object detection," in *Proceedings of the European Conference on Computer Vision*. Springer, 2020.

[132] Zhou Huang, Huai-Xin Chen, Tao Zhou, Yun-Zhi Yang, and Chang-Yin Wang, "Multi-level cross-modal interaction network for rgb-d salient object detection," *arXiv preprint arXiv:2007.14352*, 2020.

[133] Xuehao Wang, Shuai Li, Chenglizhao Chen, Yuming Fang, Aimin Hao, and Hong Qin, "Data-level recombination and lightweight fusion scheme for rgb-d salient object detection," *IEEE Transactions on Image Processing*, 2020.

[134] Xuehao Wang, Shuai Li, Chenglizhao Chen, Aimin Hao, and Hong Qin, "Knowing depth quality in advance: A depth quality assessment method for rgb-d salient object detection," *arXiv preprint arXiv:2008.04157*, 2020.

[135] Chenglizhao Chen, Jipeng Wei, Chong Peng, and Hong Qin, "Depth quality aware salient object detection," *IEEE Transactions on Image Processing*, 2020.

[136] Jiawei Zhao, Yifan Zhao, Jia Li, and Xiaowu Chen, "Is depth really necessary for salient object detection," in *ACM Multimedia*, 2020.

[137] Hao Chen, Yongjian Deng, Youfu Li, Tzu-Yi Hung, and Guosheng Lin, "Rgbd salient object detection via disentangled cross-modal fusion," *IEEE Transactions on Image Processing*, vol. 29, pp. 8407–8416, 2020.

[138] Yuzhen Niu, Yujie Geng, Xueqing Li, and Feng Liu, "Leveraging stereopsis for saliency analysis," in *Proceedings of the IEEE Conference on Computer Vision and Pattern Recognition*. IEEE, 2012, pp. 454–461.

[139] Nianyi Li, Jinwei Ye, Yu Ji, Haibin Ling, and Jingyi Yu, "Saliency detection on light field," in *Proceedings of the IEEE Conference on Computer Vision and Pattern Recognition*, 2014, pp. 2806–2813.

[140] yu Zhang et al., "Feature reintegration over differential treatment: A top-down and adaptive fusion network for rgb-d salient object detection," in *ACM Multimedia*, 2020.

[141] Nianyi Li, Bilin Sun, and Jingyi Yu, "A weighted sparse coding framework for saliency detection," in *Proceedings of the IEEE Conference on Computer Vision and Pattern Recognition*, 2015, pp. 5216–5223.

[142] Jun Zhang, Meng Wang, Jun Gao, Yi Wang, Xudong Zhang, and Xindong Wu, "Saliency detection with a deeper investigation of light field.," in *Proceedings of the International Joint Conference on Artificial Intelligence*, 2015, pp. 2212–2218.

[143] Hao Sheng, Shuo Zhang, Xiaoyu Liu, and Zhang Xiong, "Relative location for light field saliency detection," in *Proceedings of the IEEE Conference on Acoustics, Speech and Signal Processing*. IEEE, 2016, pp. 1631–1635.

[144] Jun Zhang, Meng Wang, Liang Lin, Xun Yang, Jun Gao, and Yong Rui, "Saliency detection on light field: A multi-cue approach," *ACM Transactions on Multimedia Computing, Communications, and Applications*, vol. 13, no. 3, pp. 1–22, 2017.

[145] Anzhi Wang, Minghui Wang, Xiaoyan Li, Zetian Mi, and Huan Zhou, "A two-stage bayesian integration framework for salient object detection on light field," *Neural Processing Letters*, vol. 46, no. 3, pp. 1083–1094, 2017.

[146] Nianyi Li, Jinwei Ye, Yu Ji, Haibing Ling, and Jingyi Yu, "Saliency detection on light field," *IEEE Transactions on Pattern Analysis and Machine Intelligence*, vol. 39, no. 8, pp. 1605–1616, 2017.

[147] Chao Li, Bin Zhan, Shuo Zhang, and Hao Sheng, "Saliency detection with relative location measure in light field image," in *Proceedings of the International Conference on Image, Vision and Computing*. IEEE, 2017, pp. 8–12.

[148] Shizheng Wang, Wenjuan Liao, Phil Surman, Zhigang Tu, Yuanjin Zheng, and Junsong Yuan, "Salience guided depth calibration for perceptually optimized compressive light field 3d display," in *Proceedings of the IEEE Conference on Computer Vision and Pattern Recognition*, 2018, pp. 2031–2040.

[149] Yongri Piao, Xiao Li, and Miao Zhang, "Depth-induced cellular automata for light field saliency," in *Frontiers in Optics*. Optical Society of America, 2018, pp. FTh3E–3.

[150] Tiantian Wang, Yongri Piao, Xiao Li, Lihe Zhang, and Huchuan Lu, "Deep learning for light field saliency detection," in *Proceedings of the IEEE International Conference on Computer Vision*, 2019, pp. 8838–8848.

[151] Yongri Piao, Zhengkun Rong, Miao Zhang, Xiao Li, and Huchuan Lu, "Deep light-field-driven saliency detection from a single view," in *Proceedings of the International Joint Conference on Artificial Intelligence*, 2019.

[152] Miao Zhang, Jingjing Li, JI WEI, Yongri Piao, and Huchuan Lu, "Memory-oriented decoder for light field salient object detection," in *Proceedings of the International Conference on Neural Information Processing Systems*, 2019, pp. 896–906.

[153] Yongri Piao, Zhengkun Rong, Miao Zhang, and Huchuan Lu, "Exploit and replace: An asymmetrical two-stream architecture for versatile light field saliency detection," in *Proceedings of the Association for the Advancement of Artificial Intelligence*, 2020.

[154] Xue Wang, Yingying Dong, Qi Zhang, and Qing Wang, "Region-based depth feature descriptor for saliency detection on light field," *Multimedia Tools and Applications*, 2020.

[155] Miao Zhang, Wei Ji, Yongri Piao, Jingjing Li, Yu Zhang, Shuang Xu, and Huchuan Lu, "Lfnet: Light field fusion network for salient object detection," *IEEE Transactions on Image Processing*, vol. 29, pp. 6276–6287, 2020.

[156] Jun Zhang, Yamei Liu, Shengping Zhang, Ronald Poppe, and Meng Wang, "Light field saliency detection with deep convolutional networks," *IEEE Transactions on Image Processing*, vol. 29, pp. 4421–4434, 2020.

[157] Radhakrishna Achanta, Sheila Hemami, Francisco Estrada, and Sabine Susstrunk, "Frequency-tuned salient region detection," in *Proceedings of the IEEE conference on Computer Vision and Pattern Recognition*. IEEE, 2009, pp. 1597–1604.

[158] Federico Perazzi, Philipp Krähenbühl, Yael Pritch, and Alexander Hornung, "Saliency filters: Contrast based filtering for salient region detection," in *Proceedings of the IEEE Conference on Computer Vision and Pattern Recognition*. IEEE, 2012, pp. 733–740.

[159] Deng-Ping Fan, Ming-Ming Cheng, Yun Liu, Tao Li, and Ali Borji, "Structure-measure: A new way to evaluate foreground maps," in *Proceedings of the IEEE International Conference on Computer Vision*, 2017, pp. 4548–4557.

[160] Deng-Ping Fan, Cheng Gong, Yang Cao, Bo Ren, Ming-Ming Cheng, and Ali Borji, "Enhanced-alignment measure for binary foreground map evaluation," in *Proceedings of the International Joint Conferences on Artificial Intelligence*, 2018, pp. 698–704.

[161] Yao Qin, Huchuan Lu, Yiqun Xu, and He Wang, "Saliency detection via cellular automata," in *Proceedings of the IEEE Conference on Computer Vision and Pattern Recognition*, 2015, pp. 110–119.

[162] Li Zhou, Zhaohui Yang, Qing Yuan, Zongtan Zhou, and Dewen Hu, "Salient region detection via integrating diffusion-based compactness and local contrast," *IEEE Transactions on Image Processing*, vol. 24, no. 11, pp. 3308–3320, 2015.

[163] Xiaoming Huang and Yu-Jin Zhang, "300-fps salient object detection via minimum directional contrast," *IEEE Transactions on Image Processing*, vol. 26, no. 9, pp. 4243–4254, 2017.

[164] Fang Huang, Jinqing Qi, Huchuan Lu, Lihe Zhang, and Xiang Ruan, "Salient object detection via multiple instance learning," *IEEE Transactions on Image Processing*, vol. 26, no. 4, pp. 1911–1922, 2017.

[165] Xiaoming Huang and Yujin Zhang, "Water flow driven salient object detection at 180 fps," *Pattern Recognition*, vol. 76, pp. 95–107, 2018.

[166] Chang Xu, Dacheng Tao, and Chao Xu, "Multi-view learning with incomplete views," *IEEE Transactions on Image Processing*, vol. 24, no. 12, pp. 5812–5825, 2015.

[167] Tao Zhou, Kim-Han Thung, Xiaofeng Zhu, and Dinggang Shen, "Effective feature learning and fusion of multimodality data using stage-wise deep neural network for dementia diagnosis," *Human Brain Mapping*, vol. 40, no. 3, pp. 1001–1016, 2019.

[168] Tao Zhou, Mingxia Liu, Kim-Han Thung, and Dinggang Shen, "Latent representation learning for alzheimer's disease diagnosis with incomplete multi-modality neuroimaging and genetic data," *IEEE Transactions on Medical Imaging*, vol. 38, no. 10, pp. 2411–2422, 2019.

[169] Tao Zhou, Kim-Han Thung, Mingxia Liu, Feng Shi, Changqing Zhang, and Dinggang Shen, "Multi-modal latent space inducing ensemble svm classifier for early dementia diagnosis with neuroimaging data," *Medical Image Analysis*, vol. 60, pp. 101630, 2020.

[170] Tao Zhou, Huazhu Fu, Geng Chen, Jianbing Shen, and Ling Shao, "Hi-net: hybrid-fusion network for multi-modal MR image synthesis," *IEEE Transactions on Medical Imaging*, vol. 39, no. 9, pp. 2772–2781, 2020.

[171] Clément Godard, Oisin Mac Aodha, and Gabriel J Brostow, "Unsupervised monocular depth estimation with left-right consistency," in *Proceedings of the IEEE Conference on Computer Vision and Pattern Recognition*, 2017, pp. 270–279.

[172] Fayao Liu, Chunhua Shen, and Guosheng Lin, "Deep convolutional neural fields for depth estimation from a single image," in *Proceedings of the IEEE Conference on Computer Vision and Pattern Recognition*, 2015, pp. 5162–5170.

[173] Lijun Wang, Jianming Zhang, Oliver Wang, Zhe Lin, and Huchuan Lu, "Sdc-depth: Semantic divide-and-conquer network for monocular depth estimation," in *Proceedings of the IEEE Conference on Computer Vision and Pattern Recognition*, 2020, pp. 541–550.

[174] Lei Jin, Yanyu Xu, Jia Zheng, Junfei Zhang, Rui Tang, Shugong Xu, Jingyi Yu, and Shenghua Gao, "Geometric structure based and regularized depth estimation from 360 indoor imagery," in *Proceedings of the IEEE Conference on Computer Vision and Pattern Recognition*, 2020, pp. 889–898.

[175] Mehdi Mirza and Simon Osindero, "Conditional generative adversarial nets," *arXiv preprint arXiv:1411.1784*, 2014.

[176] Dandan Zhu, Lei Dai, Ye Luo, Guokai Zhang, Xuan Shao, Laurent Itti, and Jianwei Lu, "Multi-scale adversarial feature learning for saliency detection," *Symmetry*, vol. 10, no. 10, pp. 457, 2018.

[177] Junting Pan, Cristian Canton Ferrer, Kevin McGuinness, et al., "Salgan: Visual saliency prediction with generative adversarial networks," *arXiv preprint arXiv:1701.01081*, 2017.

[178] Ashish Vaswani, Noam Shazeer, Niki Parmar, Jakob Uszkoreit, Llion Jones, Aidan N Gomez, Łukasz Kaiser, and Illia Polosukhin, "Attention is all you need," in *Proceedings of the Conference on Neural Information Processing Systems*, 2017, pp. 5998–6008.

[179] Fei Wang, Mengqing Jiang, Chen Qian, Shuo Yang, Cheng Li, Honggang Zhang, Xiaogang Wang, and Xiaoou Tang, "Residual attention network for image classification," in *Proceedings of the IEEE Conference on Computer Vision and Pattern Recognition*. Springer, 2017, pp. 3156–3164.

[180] Hao-Shu Fang, Jinkun Cao, Yu-Wing Tai, and Cewu Lu, "Pairwise body-part attention for recognizing human-object interactions," in *Proceedings of the European Conference on Computer Vision*. Springer, 2018, pp. 51–67.

[181] Wenguan Wang and Jianbing Shen, "Deep visual attention prediction," *IEEE Transactions on Image Processing*, vol. 27, no. 5, pp. 2368–2378, 2017.

[182] Jiasen Lu, Jianwei Yang, Dhruv Batra, and Devi Parikh, "Hierarchical question-image co-attention for visual question answering," in *Proceedings of the International Conference on Neural Information Processing Systems*, 2016, pp. 289–297.

[183] Zhou Yu, Jun Yu, Yuhao Cui, Dacheng Tao, and Qi Tian, "Deep modular co-attention networks for visual question answering," in *Proceedings of the IEEE Conference on Computer Vision and Pattern Recognition*, 2019, pp. 6281–6290.

[184] Xiankai Lu, Wenguan Wang, Chao Ma, Jianbing Shen, Ling Shao, and Fatih Porikli, "See more, know more: Unsupervised video object segmentation with co-attention siamese networks," in *Proceedings of the IEEE Conference on Computer Vision and Pattern Recognition*, 2019, pp. 3623–3632.

[185] Yu Zeng, Yunzhi Zhuge, Huchuan Lu, Lihe Zhang, Mingyang Qian, and Yizhou Yu, "Multi-source weak supervision for saliency detection," in *Proceedings of the IEEE Conference on Computer Vision and Pattern Recognition*, 2019, pp. 6074–6083.

[186] Dingwen Zhang, Deyu Meng, Long Zhao, and Junwei Han, "Bridging saliency detection to weakly supervised object detection based on self-paced curriculum learning," *arXiv preprint arXiv:1703.01290*, 2017.

[187] Mingyang Qian, Jinqing Qi, Lihe Zhang, Mengyang Feng, and Huchuan Lu, "Language-aware weak supervision for salient object detection," *Pattern Recognition*, vol. 96, pp. 106955, 2019.

[188] Pengxiang Yan, Guanbin Li, Yuan Xie, Zhen Li, Chuan Wang, Tianshui Chen, and Liang Lin, "Semi-supervised video salient object detection using pseudo-labels," in *Proceedings of the IEEE International Conference on Computer Vision*, 2019, pp. 7284–7293.

[189] Yuan Zhou, Shuwei Huo, Wei Xiang, Chunping Hou, and Sun-Yuan Kung, "Semi-supervised salient object detection using a linear feedback control system model," *IEEE Transactions on Cybernetics*, vol. 49, no. 4, pp. 1173–1185, 2018.

[190] Dingwen Zhang, Junwei Han, and Yu Zhang, "Supervision by fusion: Towards unsupervised learning of deep salient object detector," in *Proceedings of the IEEE International Conference on Computer Vision*, 2017, pp. 4048–4056.

[191] Tianlong Chen, Sijia Liu, Shiyu Chang, Yu Cheng, Lisa Amini, and Zhangyang Wang, "Adversarial robustness: From self-supervised pre-training to fine-tuning," in *Proceedings of the IEEE Conference on Computer Vision and Pattern Recognition*, 2020, pp. 699–708.

[192] Angela Dai, Christian Diller, and Matthias Nießner, "Sg-nn: Sparse generative neural networks for self-supervised scene completion of rgb-d scans," in *Proceedings of the IEEE Conference on Computer Vision and Pattern Recognition*, 2020, pp. 849–858.

[193] Kevin Lai, Liefeng Bo, Xiaofeng Ren, and Dieter Fox, "A large-scale hierarchical multi-view rgb-d object dataset," in *Proceedings of the IEEE International Conference on Robotics and Automation*. IEEE, 2011, pp. 1817–1824.

[194] Jing Zhang, Wanqing Li, Pichao Wang, Philip Ogunbona, Song Liu, and Chang Tang, "A large scale rgb-d dataset for action recognition," in *Proceedings of the International Workshop on Understanding Human Activities through 3D Sensors*. Springer, 2016, pp. 101–114.

[195] Yihui He, Ji Lin, Zhijian Liu, Hanrui Wang, Li-Jia Li, and Song Han, "Amc: Automl for model compression and acceleration on mobile devices," in *Proceedings of the European Conference on Computer Vision*. Springer, 2018, pp. 784–800.

[196] Yu Cheng, Duo Wang, Pan Zhou, and Tao Zhang, "A survey of model compression and acceleration for deep neural networks," *arXiv preprint arXiv:1710.09282*, 2017.

[197] Yunpeng Ma, Dengdi Sun, Qianqian Meng, Zhuanlian Ding, and Chenglong Li, "Learning multiscale deep features and svm regressors for adaptive rgb-t saliency detection," in *Proceedings of the International Symposium on Computational Intelligence and Design*. IEEE, 2017, vol. 1, pp. 389–392.

[198] Chenglong Li, Guizhao Wang, Yunpeng Ma, Aihua Zheng, Bin Luo, and Jin Tang, "A unified rgb-t saliency detection benchmark: dataset, baselines, analysis and a novel approach," *arXiv preprint arXiv:1701.02829*, 2017.

[199] Guizhao Wang, Chenglong Li, Yunpeng Ma, Aihua Zheng, Jin Tang, and Bin Luo, "Rgb-T saliency detection benchmark: Dataset, baselines, analysis and a novel approach," in *Proceedings of the Chinese Conference on Image and Graphics Technologies*. Springer, 2018, pp. 359–369.

[200] Dengdi Sun, Sheng Li, Zhuanlian Ding, and Bin Luo, "Rgb-t saliency detection via robust graph learning and collaborative manifold ranking," in *Proceedings of the International Conference on Bio-Inspired Computing: Theories and Applications*. Springer, 2019, pp. 670–684.

[201] Zhengzheng Tu, Tian Xia, Chenglong Li, Yijuan Lu, and Jin Tang, "M3s-nir: Multi-modal multi-scale noise-insensitive ranking for rgb-t saliency detection," in *Proceedings of the IEEE Conference on Multimedia Information Processing and Retrieval*. IEEE, 2019, pp. 141–146.

[202] Zhengzheng Tu, Zhun Li, Chenglong Li, Yang Lang, and Jin Tang, "Multi-interactive encoder-decoder network for rgbt salient object detection," *arXiv preprint arXiv:2005.02315*, 2020.

[203] Zhengzheng Tu, Tian Xia, Chenglong Li, Xiaoxiao Wang, Yan Ma, and Jin Tang, "Rgb-t image saliency detection via collaborative graph learning," *IEEE Transactions on Multimedia*, vol. 22, no. 1, pp. 160–173, 2019.

[204] Qiang Zhang, Nianchang Huang, Lin Yao, Dingwen Zhang, Caifeng Shan, and Jungong Han, "Rgb-t salient object detection via fusing multi-level cnn features," *IEEE Transactions on Image Processing*, vol. 29, pp. 3321–3335, 2019.

[205] Zhengzheng Tu, Yan Ma, Zhun Li, Chenglong Li, Jieming Xu, and Yongtao Liu, "Rgbt salient object detection: A large-scale dataset and benchmark," *arXiv preprint arXiv:2007.03262*, 2020.